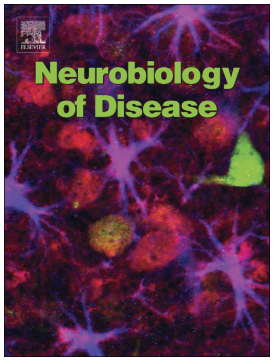

Chronic stress-induced gut dysfunction exacerbates Parkinson's disease phenotype and pathology in a rotenone-induced mouse model of Parkinson's disease

Hemraj B. Dodiya, Christopher B. Forsyth, Robin M. Voigt, Phillip A. Engen, Jinal Patel, Maliha Shaikh, Stefan J. Green, Ankur Naqib, Avik Roy, Jeffrey H. Kordower, Kalipada Pahan, Kathleen M. Shannon, Ali Keshavarzian

PII: S0969-9961(18)30768-X
DOI: https://doi.org/10.1016/j.nbd.2018.12.012
Reference: YNBDI 4352

To appear in: *Neurobiology of Disease*

Received date: 12 June 2018
Revised date: 19 November 2018
Accepted date: 19 December 2018

Please cite this article as: Hemraj B. Dodiya, Christopher B. Forsyth, Robin M. Voigt, Phillip A. Engen, Jinal Patel, Maliha Shaikh, Stefan J. Green, Ankur Naqib, Avik Roy, Jeffrey H. Kordower, Kalipada Pahan, Kathleen M. Shannon, Ali Keshavarzian , Chronic stress-induced gut dysfunction exacerbates Parkinson's disease phenotype and pathology in a rotenone-induced mouse model of Parkinson's disease. Ynbdi (2018), https://doi.org/10.1016/j.nbd.2018.12.012

Chronic Stress-induced Gut Dysfunction Exacerbates Parkinson's Disease Phenotype and pathology in a Rotenone-induced mouse model of Parkinson's Disease.

Hemraj B. Dodiya, Ph.D.[1,2], Christopher B. Forsyth, Ph.D.[2], Robin M. Voigt, Ph.D.[2], Phillip A. Engen, B.S.[2], Jinal Patel, M.S.[2], Maliha Shaikh, M.S.[2], Stefan J. Green, Ph.D.[3], Ankur Naqib, B.S.[3], Avik Roy, Ph.D.[4], Jeffrey H. Kordower, Ph.D.[4], Kalipada Pahan, Ph.D.[4], Kathleen M. Shannon, M.D.[5], Ali Keshavarzian, M.D.[2,6,*] Ali_Keshavarzian@rush.edu

[1]Department of Neurobiology, the University of Chicago, Chicago, IL USA

[2]Department of Internal Medicine, Division of Digestive Diseases, Rush University Medical Center, Chicago, IL USA

[3]Department of Biological Sciences, University of Illinois at Chicago, Chicago, IL USA

[4]Department of Neurology, Rush University Medical Center, Chicago, IL USA

[5]Department of Neurology, University of Wisconsin School of Public Health, Madison, WI USA

[6]Division of Pharmacology, Utrecht Institute for Pharmaceutical Sciences, Utrecht University, Utrecht Netherlands

[*]**Corresponding author at**: Rush University Medical Center, Department of Internal Medicine, Division of Digestive Diseases, 1725 W Harrison St, Suite 206, Chicago IL 60612.

Abstract

Recent evidence provides support for involvement of the microbiota-gut-brain axis in Parkinson's disease (PD) pathogenesis. We propose that a pro-inflammatory intestinal milieu, due to intestinal hyper-permeability and/or microbial dysbiosis, initiates or exacerbates PD pathogenesis. One factor that can cause intestinal hyper-permeability and dysbiosis is chronic stress which has been shown to accelerate neuronal degeneration and motor deficits in Parkinsonism rodent models. We hypothesized that stress-induced intestinal barrier dysfunction and microbial dysbiosis lead to a pro-inflammatory milieu that exacerbates the PD phenotype in the low-dose oral rotenone PD mice model. To test this hypothesis, mice received unpredictable restraint stress (RS) for 12 weeks, and during the last six weeks mice also received a daily administration of low-dose rotenone (10mg/kg/day) orally. The initial six weeks of RS caused significantly higher urinary cortisol, intestinal hyperpermeability, and decreased abundance of putative "anti-inflammatory" bacteria (*Lactobacillus*) compared to non-stressed mice. Rotenone alone (i.e., without RS) disrupted the colonic expression of the tight junction protein ZO-1, increased oxidative stress (N-tyrosine), increased myenteric plexus enteric glial cell GFAP expression and increased α-synuclein (α-syn) protein levels in the colon compared to controls. Restraint stress exacerbated these rotenone-induced changes. Specifically, RS potentiated rotenone-induced effects in the colon including: 1) intestinal hyper-permeability, 2) disruption of tight junction proteins (ZO-1, Occludin, Claudin1), 3) oxidative stress (N-tyrosine), 4) inflammation in glial cells (GFAP + enteric glia cells), 5) α-syn, 6) increased relative abundance of fecal *Akkermansia* (mucin-degrading Gram-negative bacteria), and 7) endotoxemia. In addition, RS promoted a number of rotenone-induced effects in the brain including: 1) reduced number of resting microglia and a higher number of dystrophic/phagocytic microglia as well as

(FJ-C+) dying cells in the substantia nigra (SN), 2) increased lipopolysaccharide (LPS) reactivity in the SN, and 3) reduced dopamine (DA) and DA metabolites (DOPAC, HVA) in the striatum compared to control mice. Our findings support a model in which chronic stress-induced, gut-derived, pro-inflammatory milieu exacerbates the PD phenotype via a dysfunctional microbiota-gut-brain axis.

Keywords: Microbiota-gut-brain axis, intestinal hyper-permeability, microbiome dysbiosis, peripheral inflammation, Parkinson's disease, intestinal barrier, rodent behavior, neurodegenerative disease.

Introduction

The etiology of Parkinson's disease (PD) is not clear but evidence strongly suggests that chronic neuroinflammation is a factor contributing to neurodegeneration.[1-7] The underlying source of the neuroinflammation is unknown; but recent observational studies in PD patients and experimental studies provide compelling evidence for a gut-derived, pro-inflammatory state as an important source for neuroinflammation and neurodegeneration in PD.[8-14] For example, newly diagnosed PD patients exhibit intestinal hyperpermeability and endotoxemia, as well as gut microbiota dysbiosis (i.e., an abnormal intestinal microbiota composition and function).[12, 14] While this finding cannot distinguish between disease cause and effect, it does provide a strong rationale to investigate the hypothesis that gut-derived inflammation, due to intestinal hyper-permeability or dysbiosis, promotes neuroinflammation and neurodegenerative changes relevant to PD pathogenesis.

If the gut is promoting PD pathogenesis then factors that cause gut leakiness to endotoxins and/or dysbiosis should exacerbate PD-associated pathologies and the phenotype. One such environmental factor is chronic stress. Indeed, several animal and human studies have shown that chronic stress promotes both intestinal hyperpermeability and dysbiosis.[15-20] Compelling data suggest that patients with PD experience a high level of stress[21, 22] with PD patients having higher cortisol levels than healthy controls.[23] Despite these data, it is not clear if stress-induced intestinal hyper-permeability or dysbiosis is important in the pathogenesis of PD or just a consequence of PD. However, previous studies in rodents show that stress is sufficient to cause microglial activation, neuroinflammation, and loss of dopaminergic neurons in the SN.[24,25, 26] Therefore, it is possible that stress-induced effects on the gut (intestinal hyperpermeability/dysbiosis) may promote neuroinflammation and neurodegeneration.

Accordingly, we hypothesized that chronic stress causes disruption of the intestinal barrier and intestinal dysbiosis resulting in exacerbation of PD pathology. To this end, we used unpredictable chronic restraint (12 weeks) to induce stress in combination with low-dose oral rotenone (last 6 weeks) to explore dysfunctional gut-brain axis in proposed PD mice model.[27]

Results

Measures of stress parameters support the effectiveness of the chronic restraint stress (RS) protocol

The experimental protocol is outlined in Figure 1A. Four different parameters were recorded and analyzed to confirm effectiveness of RS protocol including: body weight, food consumption, fecal output, and urinary cortisol. 1) *Body Weight* (Figure 1B). Analysis of body weight data revealed a significant effect of stress on body weight (rmANOVA: (group) $F_{(1,24)}$=12.19, P=0.002; (time) $F_{(7,168)}$=12.18, P<0.0001; (interaction) $F_{(7, 168)}$=22.22, P<0.0001). Post-hoc analysis showed significantly lower body weight in the RS groups compared to controls at week 3 (P<0.01), week 5 (P<0.001), week 7 (P<0.001), week 9 (P<0.001), week 11 (P<0.01), and week 13 (P<0.001). Starting at week 9, body weight loss was noted in controls which may be a consequence of stress associated with the daily oral gavage (vehicle/rotenone) procedure. 2) *Food Intake* (Figure 1C). There were no significant differences in food intake between the control and RS groups (rmANOVA: $F_{(1,24)}$=2.325, P=0.14) nor a group and time interaction (P>0.05); however there was a significant effect of time on food intake ($F_{(4,96)}$=148.9, P<0.0001). 3) *Fecal Output* (Figure 1D). Fecal output during two-hours RS was significantly higher in the RS group compared to controls (rmANOVA: (groups) $F_{(1,24)}$=147.3, P<0.0001; (time) $F_{(13, 312)}$=10.82, P<0.0001; (interaction) $F_{(13, 312)}$=5.443, P<0.0001). Post-hoc analysis

showed significantly higher fecal output in the RS group from week 3 through week 15 (P<0.001). 4) *Urinary Cortisol* (Figure 1E). Baseline urinary cortisol levels were not significantly different (data not shown). Six weeks of RS significantly increased urinary cortisol (unpaired two-tailed t test: $t_{(12)=}$2.49, P=0.03). Taken together, these data confirm effectiveness of the unpredictable chronic RS protocol.

Restraint stress promoted rotenone-induced intestinal hyperpermeability, endotoxemia and tight junction barrier loss

Six weeks of RS significantly increased urinary excretion of sucralose/lactulose (unpaired two-tailed t test: $t_{(26)}$=3.38, P=0.002) compared to controls indicating intestinal hyperpermeability (Figure 2A). In contrast, there were no significant changes in urinary excretion of sucrose ($t_{(26)}$=0.58, P=0.570) or mannitol ($t_{(26)}$=0.13, P=0.901) (Figure S1:A, C- markers of small bowel permeability). Together these data suggest the site of disruption of intestinal barrier function is primarily colon [28].At week 15, there was still a significant effect of stress on the urinary sucralose/lactulose ratio (Figure 2B) ($F_{(1,22)}$=11.91, P<0.00) but no significant effect of rotenone nor a rotenone and stress interaction. Post-hoc analysis showed significantly increased sucralose/lactulose ratio in the RS+rotenone mice compared to rotenone mice (P<0.05). Urinary excretion of sucrose or mannitol showed no significant differences between groups (Figure S1: B, D).

Plasma LPS (Figure 2C) and plasma lipopolysaccharide binding protein (LBP) (Figure 2D) were measured at the time of sacrifice (week 15). Analysis revealed plasma LPS levels were significantly impacted by stress ($F_{(1,22)}$=4.33, P<0.05) but there was not a significant effect of rotenone nor rotenone and stress interaction. Post-hoc analysis showed significantly increased

plasma LPS levels in RS+rotenone compared to rotenone treatment alone (P<0.05). Plasma LBP levels were significantly impacted by rotenone ($F_{(1,22)}$=7.14, P=0.01) but no significant effects of stress nor was a rotenone and stress interaction observed (Figure 2D). Post-hoc analysis showed significantly higher LBP levels in RS+rotenone mice compared to RS alone (P<0.05). Together these data suggest that stress exacerbated colonic hyperpermeability and endotoxemia.

Immunofluorescence staining for the tight junction proteins zonula occludens-1 (ZO-1), occludin, and claudin-1 showed evidence of intestinal barrier dysfunction (Figure 2E). *ZO-1*. Visualization showed continuous, robust expression of ZO-1 (i.e., normal lattice structure distribution) at the epithelial lining of the control group while the rotenone group showed disrupted, non-continuous structure of ZO-1 (Figure 2E). By comparison, RS resulted in complete disappearance of ZO-1 expression at the epithelial lining irrespective of rotenone exposure (Figure 2E). Semi-quantitative analysis of the staining using an integrity scoring scale (0=no staining – 3=continuous normal expression) showed significant difference due to stress ($F_{(1,22)}$=12.57, P<0.00; Figure 2F) but no significant effect of rotenone nor a rotenone and stress interaction. Post-hoc analysis showed a significantly lower integrity score in RS compared to controls (P<0.00). *Occludin*. Microscopic analysis showed intact occludin staining in the epithelial lining of both control and rotenone-treated mice (Figure 2E). In contrast, RS reduced the expression of occludin irrespective of rotenone treatment (Figure 2E). Integrity scoring data for occludin expression showed significant effect of stress ($F_{(1,22)}$=39.38, $P<0.00$) but no significant effect of rotenone nor a rotenone by stress interaction (Figure 2G). Post-hoc analysis showed a significant difference between colonic occludin expression in RS and control mice (P<0.00), RS+rotenone compared to rotenone-treated mice (P<0.00). *Claudin 1*. Microscopic visualization showed robust expression of claudin-1 located in the colonic epithelial lining of the

control group and this expression was significantly impacted by both stress ($F_{(1,22)}$=5.71, P=0.03) and rotenone ($F_{(1,22)}$=4.56, P=0.04) but an interaction was not observed (Figure 2H). Post-hoc analysis showed significantly lower expression of claudin-1 in RS+rotenone compared to rotenone (P<0.05). These data indicate that stress and rotenone treatment affected different tight junction profiles with the RS+rotenone group showing the most prominent effects and this could explain why RS+rotenone showed a significant increase in the sucralose/lactulose ratio and markers of endotoxemia compared to RS and rotenone alone.

We also performed WB analysis on the levels of claudin1 and Occludin in tissue homogenates (n=4/5) from the colon. There were no significant differences in the protein levels of these tight junctional proteins between groups (Figure S1 E, F). It should be noted that several studies demonstrated that topography of the tight junction proteins is more critical than their protein levels for the regulation of the intestinal permeability. Indeed, abnormal redistribution of these tight junction proteins, detected by histology or immunofluorescence microscopy, is associated with abnormal intestinal permeability without any changes in their overall protein expressions (in whole GI wall or tissue lysate) in both rodents and human [29-35].

Restraint stress lowered putative "anti-inflammatory" fecal microbiota and rotenone increased the relative abundance of putative "pro-inflammatory" fecal microbiota

We assessed mouse fecal microbiota structure at baseline, week 9 (after 6 weeks of stress), and at the time of sacrifice (week 15) (Figure 1A), employing alpha and beta diversity analyses.

Baseline. At baseline, very small but significant differences in fecal microbial community structure were observed between RS and control group animals (Table 1, Figure 3A, Figure

S2A). Specifically, the RS group had significantly different alpha diversity compared to the control group at multiple taxonomic levels (RS higher than control group: Phylum (Shannon index, Simpson index, evenness), Family (evenness); RS lower than the control group Family (richness)) (Table 1). Analysis of similarity (ANOSIM) revealed a significant difference in alpha diversity at baseline (Global R=0.128; *P*=0.028) (Table S1). Despite these difference in alpha diversity at baseline, there were no significant differences between individual taxa at the phylum, family, or genus taxonomic levels (FDR *P*<0.05) between RS and control groups (Table S2).

Six (6) weeks of stress. At week 9, following six weeks of RS, there were no significant differences in alpha diversity between control and RS mice (Table 1), similar to results observed by others.[36] Additionally, the overall microbial community were statistically indistinguishable between RS and controls groups, at the phylum, family, and genus taxonomic levels (ANOSIM Global R=0.020, *P*=0.267) (Table S1, Figure S2B). However, examination of individual taxa between groups revealed that the relative abundance of one family and two genera were statistically different between control and RS mice after six weeks of stress (Table 2). Specifically, the relative abundance of family Lactobacillaceae and genus *Lactobacillus* were decreased (*P*<0.05) in RS mice (Figure 3B); whereas the relative abundance of bacteria in genus *Lachnospiraceae;Unclassified* was significantly increased by RS (FDR-*P*=0.02) compared to control mice (Table 2), similar to results obtained by other groups.[36] Using a predicative assessment of the microbial community functional potential (PICRUSt), we identified three metabolic pathways that were decreased by RS (Table S3). This could suggest that stress impacts host's metabolism, as evident by the RS mice in this study not gaining weight (Figure 1D). We acknowledge that the PICRUSt analyses only infer microbiota function and our results must be confirmed by the metabolomics and metagenomics in the future studies.

Twelve (12) weeks of stress. At the time of sacrifice (week 15), significant group differences were observed in alpha diversity at the taxonomic level of phylum (Table 1). At the taxonomic level of phylum, there was a significant effect of rotenone on the Shannon Index ($F_{(1,24)}$=8.47, *P*=0.01), the Simpson Index ($F_{(1, 24)}$=8.77, *P*=0.01) and evenness ($F_{(1, 24)}$=7.92, *P*=0.01), but no significant effects from stress nor a rotenone by stress interaction. Post-hoc analysis showed Shannon index (RS vs. RS+rotenone, rotenone vs. RS; *P*<0.05), Simpson index (RS vs. RS+rotenone; *P*<0.05) and evenness (RS vs. RS+rotenone, rotenone vs. RS; *P*<0.05) (Table 1 & Figure S2D). Additionally, there was a significant rotenone by stress interaction observed for evenness ($F_{(1,24)}$=4.376, *P*=0.047), at the family taxonomic level. Post-hoc comparison showed no significant differences. When analyzing the beta diversity between the mice groups at week 15, there were significant differences in the overall microbial community at all taxonomic levels between control and RS groups (ANOSIM genus: *R*=0.393; *P*=0.010), as well as between RS and RS+rotenone groups (ANOSIM genus: *R*=0.288; *P*=0.011) (Table S1). Compared to control mice, the RS group had an increased relative abundance of family Unclassified Clostridiales (*P*=0.03) (Table 3). However, the decrease in relative abundance of genus *Lactobacillus* in RS mice compared to control mice at week 9, was not observed at week 15. This finding may be the consequence of stress in the control mice due to daily oral gavage of vehicle starting at week 9. Additionally, PICRUSt analysis inferred that RS mice had decreased functional pathway relative abundances in both flavonoid (anti-inflammatory molecules) and degradation of DTT toxins, compared to control mice (Table S3). This data suggest that stress increases the likelihood of susceptibility for environmental toxins, such as rotenone, due to the gut microbiota.

Rotenone+RS-Induced Effects. Although no taxa were significantly different between rotenone-treated and control mice using stringent FDR-*P* criteria, a less stringent statistical approach did show that rotenone-treated mice had decreased relative abundance of phylum Actinobacteria (*P*=0.04) compared to controls (Table 3, Figure S2C). In contrast, the combination of RS+rotenone treatment resulted in significant changes in the intestinal microbiota (Table 3). These significant differences included: decreased relative abundance of phyla Firmicutes (FDR-*P*=0.01) and Actinobacteria (FDR-*P*=0.02) and an increased relative abundance of Verrucomicrobia (FDR-*P*=0.04) in the RS+rotenone mice compared to RS alone. At the family taxonomic level, we observed significantly decreased relative abundance in Coriobacteriaceae (FDR-*P*=0.03) and trends of decreased relative abundance of Unclassified Clostridiales (*P*=0.04), as well as trends for increased relative abundance of Verrucomicrobiaceae (*P*=0.03) and genus *Akkermansia* (*P*=0.03) in the RS+rotenone compared to RS alone. PICRUSt inferred increased relative abundance in Lipopolysaccharide-biosynthesis, Lipopolysaccharide-protein, ubiquinone system + biosynthesis, and bacterial secretion pathways in the fecal microbiota of RS+rotenone compared to RS alone (Table S3). These putative "pro-inflammatory" pathways have been detected in human Parkinson's disease and multiple systems atrophy fecal microbiota studies.[14, 37]

Gram Negative Bacteria. To explore the possibility that endotoxemia resulted from an increase in LPS producing gram-negative bacteria, we specifically investigated the relative abundance of gram-negative bacterial genera *Desulfovibrio, Bacteroides,* and *Akkermansia* (Figure 3C). We only included detected gram-negative bacteria at genus taxonomy for this comparison. These taxa showed no significant differences at baseline nor after six weeks of stress. However, the relative abundance of *Akkermansia* was significantly impacted by rotenone-

treatment ($F_{(1,24)}$=9.78, P<0.00) and stress ($F_{(1,24)}$=5.18, P=0.03), but no rotenone by stress interaction was observed. Post-hoc analysis showed significantly increased relative abundance of *Akkermansia* in RS+rotenone group compared to RS (P<0.05). No significant differences were observed in the other examined gram-negative taxa.

Firmicutes/Bacteroidetes Ratio. Next, we examined the Firmicutes/Bacteroidetes (F/B) ratio between groups. The most common bacteria in human microbiota are gram-positive Firmicutes and gram-negative Bacteroidetes[38] and several studies have analyzed the ratio of relative abundance of F/B as an important marker of the disruption of microbiota community structure and one of the microbiota parameter associated with gut health.[39-41] We found no significant differences in F/B ratio at baseline or after 6 weeks of RS. At the time of sacrifice (week 15), stress showed a significant effect on the F/B ratio ($F_{(1, 24)}$=4.322, P=0.048) (Figure 3D), but no significant effect of rotenone nor interaction. Post-hoc analysis showed no significant differences between any groups.

This data again showed that stress significantly affected microbiota community structure.

Short chain fatty acids (SCFA). We also evaluated the levels SCFA in the fecal pellets of these mice groups at the time of sacrifice (week 15) (Figure 3E-G). There was a significant effect of stress on the SCFA butyrate in the stool ($F_{(1, 21)}$=5.706, P=0.026), but no significant effects of rotenone nor an interaction (Figure 3E). Post-hoc analysis showed no significant differences between any other groups. Levels of the SCFA acetate (Figure 3F) and the SCFA propionate (Figure 3G) showed no significant changes. These data suggest that RS specifically decreased the SCFA butyrate level and this could contribute to stress-induced disruption of intestinal barrier and pro-inflammatory state because butyrate is critical in maintaining normal barrier function [42-44] and low butyrate is associated with pro-inflammatory state [45].

Stress and rotenone treatment cause oxidative stress and inflammation in colon

Gross colonic morphology was evaluated using hematoxylin and eosin (H&E) stained slides (Figure 4A). Overall, rotenone and RS mice resulted in increased immune cells infiltration in the lamina propria while RS+Rotenone resulted in even higher immune cells infiltration in the lamina propria. We next evaluated oxidative stress and inflammation in the colonic lamina propria (LP) and myenteric plexuses (MP).

n-Tyrosine reactivity in lamina propria (LP). These data were analyzed in two different ways: staining intensity (i.e., optical density (OD)) and the number of n-tyrosine positive cells in lamina propria (LP). Immunofluorescence staining for the oxidative stress marker n-tyrosine (Figure 4B) showed higher intensity of n-tyrosine staining intensity throughout the lamina propria of the rotenone-treated mice; while RS group showed increased n-tyrosine+ cells in the lamina propria. OD analysis of n-tyrosine staining intensity revealed a significant rotenone by stress interaction ($F_{(1,20)}$=6.25, P=0.02, Figure 4C) but no main effects of stress nor rotenone (P>0.05). Post-hoc comparison showed significantly higher n-tyrosine intensity in the lamina propria of rotenone-treated mice compared to controls (P<0.05). In contrast, n-tyrosine+ cell count was significantly influenced by stress ($F_{(1,20)}$=10.69, P<0.00) but not by rotenone-treatment nor a stress by rotenone interaction (p>0.05) (Figure 4D). Post-hoc comparison showed significantly higher n-tyrosine+ cells in the lamina propria of RS compared to controls (P<0.05).

Inflammation. Next we examined the impact of rotenone and/or stress on the levels of the pro-inflammatory cytokine IL-1β (Figure 4E) and enteric glial cell activity (glial fibrillary acidic protein (GFAP) + cells; Figure 4F, G, H) in colonic tissue. *Cytokine levels in tissue homogenates.* Levels of IL-1β were significantly increased by stress ($F_{(1,22)}$=9.08, P=0.01) but

there were no effects of rotenone nor a rotenone by stress interaction ($p>0.05$). Post-hoc analysis showed IL-1β levels were significantly increased by RS compared to control ($P<0.05$). To further determine whether rotenone and stress results in colonic inflammatory state, we measured additional cytokines and chemokines in the colonic tissue homogenates using Raybiotech mouse cytokine array kit. Array membranes were probed with pooled (n=3/4 per group) colon tissue homogenates (300µg of total protein lysate). Immunoblotting protocol was followed as per manufacturer's suggestion and OD values were generated from densitometric analysis to detect the levels of 22 cytokines/chemokines. Overall, RS colonic homogenates showed higher cytokines/chemokines compared to all other groups (Figure S3 A, B). Specifically, IL-9 ($P=0.038$) and IFN-gamma ($P=0.033$) levels showed statistically higher levels in RS group compared to control (stress: $F_{(1, 4)}=15.24$, $P=0.0175$, stress by rotenone interaction: $F_{(1,4)}=17.92$, $P=0.013$ respectively) (Figure S3 B).

GFAP+ enteric glia cells reactivity in lamina propria (LP) and myenteric plexuses (MP). Immunofluorescence staining showed different pattern of GFAP+ enteric glia reactivity in the lamina propria and myenteric plexuses (MP) of the colon tissue. **First,** GFAP distribution was characterized in the lamina propria (Figure 4G) as mucosal enteric glia cells/projections are known to play crucial roles in barrier integrity health and regulating immune responses in the mucosa.[46-50] OD analysis of GFAP positive enteric glia cells in the lamina propria showed a significant rotenone by stress interaction ($F_{(1,22)}=5.43$, $P=0.03$) (Figure 4G) but no main effects of rotenone or stress alone were observed ($P>0.05$). Post-hoc analysis showed significantly less GFAP intensity in the lamina propria of rotenone-treated mice compared to controls ($P<0.05$) and RS-treated mice compared to controls ($P<0.05$) (Figure 4E). **Second,** we characterized GFAP expression in the myenteric plexuses (Figure 4H). A higher enteric glial reactivity

(GFAP+ cells) in the myenteric plexuses is a sign of enteric inflammation. OD analysis of GFAP expression in the myenteric plexuses showed significant effects of stress ($F_{(1,22)}$=17.49, P<0.00) and rotenone ($F_{(1,22)}$=53.49, P<0.00), but no interaction was observed (p>0.05). Post-hoc comparison revealed significantly higher GFAP intensity in rotenone-treated mice compared to controls (P<0.00), RS compared to controls (P<0.05), RS+rotenone compared to RS (P<0.00), and RS+rotenone compared to rotenone (P<0.05).

Alpha-synuclein reactivity in myenteric plexuses (MP). Next we evaluated the effects of stress and/or rotenone on PD-like pathology in the colonic myenteric plexuses (Figure 4F, I), specifically α-synuclein (α-syn). Rotenone-treated mice had higher α-syn level compared to controls. OD analysis showed significant effects of rotenone ($F_{(1,22)}$=21.17, *P*<0.00) but no effect of stress nor was there a stress by rotenone interaction (p>0.05). Post-hoc analyses showed significantly higher α-syn in the myenteric plexuses of rotenone-treated mice compared to control mice (p<0.01) and RS+rotenone treated mice compared to RS group (p<0.05).

Restraint stress in combination with rotenone promotes neuroinflammation in the absence of rotenone in the brain

Rotenone level in the brain. It has been reported that low dose (10mg/kg), orally administered rotenone does not reach to the brain.[27] To confirm this result, rotenone content was examined within the pooled brain regions of olfactory bulb, cortex, and rostral striatum via HPLC-MS in rotenone and RS+rotenone groups at the time of sacrifice (week 15). This analysis revealed that levels of rotenone in the brain were below the detectable range (Figure S4). Even though we found no detectable rotenone in the brain, it is still possible that rotenone effects in the brain is not from its impact on gut and is due to systemic absorption of the rotenone leading

to immune activation resulting in neuro-inflammation. To exclude this possibility, we measured rotenone levels in the liver tissue and found no significant changes in total rotenone content of the liver samples ($t_{(10)}$=0.950, *P*=0.364) (Table S4). Thus, the impact of stress on rotenone-induced brain dysfunction is not from increased systemic absorption of rotenone. This supports the role for disrupted gut-brain axis in our proposed Parkinsonism rodent model.

Iba+ microglia phenotype in SN. To characterize brain inflammation, we evaluated Iba1+ microglia cells. Microglial cells in the SN were analyzed based on their morphology (see Methods Section). Upon visual inspection, brain tissue from mice undergoing RS was characterized by microglia with a larger cell body with many processes that are thought to be activated microglia whereas brain tissue from rotenone-treated mice showed microglia with a large cell body with fewer processes indicative of dystrophic/phagocytic microglia (Figure 5A). Based on these morphological characteristics (Figure 5B), cell counts were estimated for microglia cells in each category (i.e., resting, activated and dystrophic/phagocytic microglia). Two-way ANOVA and followed by post-hoc analysis showed (Figure 5C, Table S5): 1) control mice had higher numbers of resting microglia compared to all other groups (rotenone and stress interaction: $F_{(1,22)}$=39.57, *P*<0.0001, post-hoc *P*<0.0001), 2) rotenone treatment increased the numbers of dystrophic/phagocytic microglia compared to control mice (for rotenone: $F_{(1, 22)}$= 25.96, *P*<0.0001, post-hoc *P*=0.0060), 3) RS significantly reduced the number of resting microglia (*P*<0.0001) and significantly increased the number of activated microglia (rotenone and stress interaction: $F_{(1,22)}$=11.13, *P*=0.003, post-hoc *P*<0.0001) compared to controls, 4) RS+rotenone had significantly fewer resting microglia compared to control and rotenone groups (*P*<0.0008), more activated microglia compared to control (*P*<0.05), and more dystrophic/phagocytic microglia compared to control and RS groups (*P*<0.01). These data

support an increased microglial-neuroinflammation in the substantia nigra of RS+rotenone treated mice (Figure 5C, Table S5).

FJ-C+ dying cells in SN. Visualization of cell death marker (FJ-C) in the SN showed a minimal number of dying cells in the control and RS groups (Figure 5D). In contrast, a higher number of dying cells were observed in the SN of RS+rotenone (Figure 5D) . Additionally, most of the FJ-C+ cells in the SN of RS+Rotenone showed positive co-localization with TH+ marker suggesting only RS+Rotenone mice showed dying dopamine cells.

LPS reactivity in SN. Visualization of bacterial endotoxin marker LPS showed no LPS+ve structures in the SN of control groups. Rotenone treatment showed some LPS reactivity in the SN. In contrast, RS and RS+rotenone groups showed higher LPS reactivity in the SN compared to controls (Figure 5E, Figure S5).

TLR4 reactivity in Striatum. Furthermore, the bacterial endotoxin ligand toll-like receptor 4 (TLR4) was also assessed in the striatum of these mice. Visualization under confocal microscope showed minimal expression of TLR4+ cells in control and rotenone-treated mice whereas higher TLR4 immunoreactivity was observed in the striatum of RS+rotenone treated mice compared to other groups (Figure S6).

TH+ dopamine cells in SN. Immunohistochemistry for TH reactivity showed fewer TH+ cells in rotenone and RS+rotenone compared to controls. Stereological analysis showed significantly lower TH+ cell in rotenone-treated mice ($F_{(1,22)}$=49.63, P<0.00) but there was no effect of stress nor a stress by rotenone interaction (P>0.05) (Figure 5E). Post-hoc analysis showed significantly fewer TH+ cells in the SN of rotenone-treated mice compared to controls (P<0.00) and fewer cells in RS+rotenone compared to RS alone (P<0.00).

Dopamine and metabolites in Striatum. Dopamine (DA) cell loss in the SN results in less DA output in the striatum due to degeneration of nigro-striatal innervation; thus, we evaluated concentrations of DA and its metabolites DOPAC and HVA in the striatum (Figure 5F,G,H). The DA concentration was significantly affected by rotenone ($F_{(1,22)}$=10.52, P<0.00), stress ($F_{(1,22)}$=8.48, P=0.01), as well as a rotenone by stress interaction ($F_{(1,22)}$=8.57, P=0.01) (Figure 5F). Post-hoc comparison showed significantly lower striatal DA in the RS+rotenone compared to all other groups (P<0.01). Levels of striatal DOPAC showed no significant changes (p>0.05) (Figure 5G). Levels of striatal HVA was significantly impacted by stress ($F_{(1,22)}$=12.46, P=0.00) but were not affected by rotenone or a stress by rotenone interaction (p>0.05). Post-hoc analyses showed significantly lower striatal HVA in RS+rotenone mice compared to rotenone-treated group (P<0.01). These data support a significantly reduced DA availability at the striatal terminals in RS+rotenone group. Visualization of TH immunohistochemistry showed prominent reduction of TH intensity in the RS+rotenone compared to the other groups (Figure S6).

Restraint stress potentiated rotenone-induced effects on behavior

There were no significant differences in rotarod performance at baseline or after six weeks of RS (week 9) (Figure 6A). There was a significant effect of interaction between time and treatments ($F_{(6,44)}$=2.654, P=0.03) as well as significant effect of matching subjects ($F_{(22,44)}$=1.982, P=0.03). A post hoc comparison showed significantly reduced rotarod performance in RS+rotenone treatment compared to RS alone (P<0.05) at week 15.

The adhesive removal test (Figure 6B) was carried out at week 14 to assess sensory and motor impairment. Performance in the adhesive removal test was significantly influenced by stress ($F_{(1,22)}$=28.59, P<0.00), rotenone ($F_{(1,22)}$= 50.63, P<0.00), as well as a stress by rotenone

interaction ($F_{(1,22)}$=18.93, P<0.00). Post-hoc analysis showed that the RS+rotenone group took significantly longer time to remove the adhesive stickers compared to RS and rotenone groups alone (P<0.00).

The hanging grip test was carried out to measure muscle strength at week 14 (Figure 6C). Muscle strength was significantly impacted by rotenone ($F_{(1,22)}$=14.39, P<0.00) but there was no effect of stress or a stress by rotenone interaction (P>0.05). Post-hoc analysis showed that RS+rotenone mice showed lack of muscle strength compared to RS alone (P<0.01).

Evidence to support gut-brain axis involvement in our proposed model

In order to better understand the interaction between periphery and central compartments, we performed a Pearson correlation between the markers of interest (Figure 7). While correlation does not equal causation, this correlation analysis does allow us to infer potential interactions. We observed significant positive correlation between dystrophic/phagocytic microglia cell counts in the SN and decreased colonic ZO-1 tight junction protein expression (r=-0.489, P=0.011, Figure 7A), increased systemic levels of LPS (r=0.523, P=0.006, Figure 7B) and increased relative abundance of *Akkermansia* (mucin degrading, Gram negative bacteria) (r=0.437, P=0.026, Figure 7C). Also, relative abundance of *Akkermansia* inversely correlated with muscle strength performance on the hanging grip test (r=-0.575, P=0.002, Figure 7D). We also observed positive correlation between fecal butyrate levels and striatal DA levels (r=0.450, P=0.024, Figure 7E).

Discussion

The current study demonstrated that stress-induced disruption of intestinal barrier integrity, dysbiosis and endotoxemia promotes microglial activation, neuro-inflammation, DA loss and the PD phenotype in rotenone model of PD and these effects were not due to increased systemic and brain exposure to the neurotoxin rotenone. Thus, to our knowledge, our study is the first to provide unique and novel compelling evidence that a dysfunctional microbiota-gut-brain axis can potentiate the PD phenotype and pathology.

Intestinal hyper-permeability can induce systemic inflammation leading to the inflammatory responses in the brain and that should further exacerbate neuronal loss in patients with PD similar to what we observed in our rotenone model. A similar intestinal hyper-permeability model driving CNS neuroinflammation has been proposed in other neuropsychological disorders like major depression.[51]

Stress negatively affects intestinal barrier function.[15, 52, 53] In agreement with this literature, we observed that chronic stress induced by six weeks of daily RS caused significant increase in urinary sucralose/lactulose ratio which is a marker of primarily increased colonic permeability [28]. This observed leakiness to LPS appeared to be due to disruption of key tight junctional proteins in colonic tissue: ZO-1, occludin, and claudin-1, similar to data observed by others.[15] Rotenone alone reduced ZO-1 integrity as reported previously by our group[54]. While stress alone and rotenone alone disrupted some of the tight junction proteins, only RS+rotenone disrupted all three major tight junction proteins which could explain why RS+rotenone caused severe enough colonic hyperpermeability to result in increased level of plasma LPS (endotoxemia). Individual tight junction protein level did not correlate with LPS level significantly. This is not necessarily surprising because disruption of single protein does not always lead to disruption of intestinal barrier severe enough to cause endotoxemia and typically

an aggregate of disruption of several tight junction proteins is required for severe enough leak to cause elevated plasma LPS.

Several studies have shown that stress impacts intestinal microbiota composition. For example, Bailey and colleagues report significantly lower levels of *Lactobacilli* following stress in non-human primates.[18] They also report that reduced abundance of certain intestinal microflora correlated with stress-indicative behaviors but did not correlate with cortisol suggesting that chronic stress-induced biological effects may not solely be due to changes in cortisol. One study showed improved behavior, cognition and biochemical aberration in the brain following oral *Lactobacillus* administration in a rodent model of chronic stress.[55] We also observed a reduction in the relative abundance of genera *Lactobacillus* following six weeks of RS; however, there was no difference in the relative abundance of genera *Lactobacillus* between RS and none- RS groups at week 15. This might be the consequence of daily gavage-induced stress from week 9 to week 15 in all groups. In addition to *Lactobacillus*, we observed an increased relative abundance of Clostridiales (family) in the RS group compared to control mice at week 15 which is in agreement with other reports.[36, 56, 57] Although Bailey and colleagues report a lower relative abundance of *Bacteroides* due to stress,[56] our data did not show any changes in the levels of *Bacteroides* with RS.

Rotenone treatment reduced the relative abundance of Actinobacteria (phylum) and Coriobactericeae (family) compared to controls. Our data suggest that RS in combination with rotenone creates an intestinal profile that is uniquely distinct from stress or rotenone alone. For example, compared to RS alone, RS+rotenone significantly reduced the relative abundance of Firmicutes and Actinobacteria and significantly increased the relative abundance of Verrucomicrobia at the phylum level. In general, the RS+rotenone microbiota profile showed

decreased putative "anti-inflammatory" bacteria as well as an increase in putative "pro-inflammatory" bacteria and these changes may contribute to neuroinflammation and neurodegeneration observed when RS and rotenone are combined.

One consequence of intestinal hyper-permeability is immune activation and oxidative stress. Indeed our data showed increased n-tyrosine+ cells in the lamina propria and enteric glial expression in the myenteric plexuses supporting the presence of pro-inflammatory state in the colon of mice with disrupted intestinal barrier integrity and hyperpermeability. While there was no additive effect of oxidative stress (n-tyrosine) due to RS+rotenone, there was evidence that the combination promoted enteric glial activation (increased GFAP reactivity) in the myenteric plexuses of the colon.

Several animal and *in vitro* studies have used LPS to promote PD phenotype.[2, 58-60] We observed increase in LPS reactivity of the SN in stress groups (RS and RS+rotenone) suggesting that endotoxemia, either due to intestinal hyper-permeability or intestinal microbiota dysbiosis, could allow bacteria/bacterial products such as endotoxins into the SN brain region critical for PD pathogenesis. Endotoxemia associated disrupted blood brain barrier (as shown [61]) could facilitate the dysfunction of the midbrain. Bloor brain barrier integrity in the future studies using techniques appropriate to test its permeability is warranted. LPS is a primary ligand for TLR4.[62, 63] Several studies have shown that stress increases TLR4 activation in the brain[64-66] and that TLR4 is elevated in the brain of PD patients[67]. It is possible that this is due to, at least in part, to stress-induced changes in gut hyperpermeability/dysbiosis and endotoxemia.[64, 65] Similar to these findings, we also observe higher TLR4 reactivity in the midbrains of stress groups. LPS is a well-characterized neurotoxin responsible for dopamine cell degeneration in the SN;[68] thus,

chronically elevated levels of systemic LPS (as shown in our study) could contribute to brain inflammation and neurodegenerative processes via a mechanism including TLR4 signaling.

The combination of RS+rotenone appears to have important consequences in the brain. For example, RS potentiated rotenone-induced effects on the number of resting microglia and DA and HVA concentration in the striatum. Similarly, activated microglia due to stress- induced higher inflammatory response and were associated with a higher rate of death of dopaminergic neurons in the SN in stress+LPS mice.[26] Functionally, we were able to observe that the adhesive removal test appeared to be most sensitive to combined effects of stress and rotenone suggesting that sensory systems could be highly impacted by stress and stress-induced gut derived pro-inflammatory state. To further support the hypothesis that gut-derived inflammation promote neuro-inflammation, we performed series of correlation analysis (Figure 7) and found that the microglia phenotype (especially dystrophic/phagocytic microglia numbers) in SN is positively correlated with markers of disrupted colonic barrier integrity, serum LPS and relative abundance of *Akkermansia*. Behaviorally, the outcomes from the adhesive removal test appear to be correlated to TH+ DA cells in the SN and DA concentration in the striatum. Our findings begin to provide evidence for a role for disrupted gut-brain axis in pathogenesis of PD. Further studies are needed to determine whether there is a causal link between gut-brain axis and PD. Our data now provide a scientific rationale for conducting longitudinal and interventional studies to look for the causal link.

The data observed in the current study support what we have observed in human PD patients. Our previously published data show that PD subjects, including newly diagnosed PD subjects, have evidence of microbial dysbiosis,[14] intestinal hyper-permeability,[12] and microbial translocation.[12, 69] The exact cause of intestinal hyperpermeability in PD patients is unknown, but

our current study suggests that events such as stress and or dysbiosis that initiate intestinal hyperpermeability may induce low-grade chronic intestinal and neuro-inflammation. This low-grade chronic inflammation could contribute to neurodegeneration as has been proposed in depression.[51] We propose that higher TLR4 expression in the peripheral blood mononuclear cells and the brains of PD patients[67] could be caused, at least in part, by intestinal dysbiosis and/or gut hyperpermeability. Future interventional clinical studiessuch as use of microbiota directed intervention, are needed to directly answer these questions and establish the causal link between gut-derived inflammation, upregulated TLR-4 signaling and neuro-inflammation in PD patients.

In summary, we have provided new evidence that stress-induced intestinal hyper-permeability and microbiota dysbiosis promote an intestinal pro-inflammatory milieu, peripheral (and SN) endotoxemia, neuroinflammation, and neurodegeneration in a low-dose, oral rotenone-induced PD mouse model. Future mechanistic studies could help further understand the exact role of stress-mediated gut dysfunction in neurodegeneration in the SN. The current study adds significant new support for the possible role of the microbiota-gut-brain axis in PD pathogenesis.

Materials and methods

Animals and experimental protocol

Young adult (6-8 weeks) male C57BL/6 mice were employed for this study. We chose to study only male mice because incidence of PD is biased towards male [70, 71]. Animals were purchased from Harlan (Indianapolis, IN). We elected to house 3 or 4 mice in each cage. The primary question for the current study was if stress exacerbates rotenone-induced PD pathology. It is now well established that housing rodents individually results in stress [72-76] compared to co-housing. Thus, we elected not to singly house mouse to avoid co-founders that would impair data interpretation. Only mice from the same experimental groups were housed together in order to avoid cross-contamination of stool microbiome that could clearly mask the microbiota-mediated readout(s) as reported in our study. Both RS and non-RS group mice were housed and handled in a specific pathogen free (SPF) environment either in the SPF mice facility or approved behavior facility room. Experimenters followed the same exact conditions, including the usage of PPE (personal protective equipment; especially hand gloves), which was changed between handling of mice from different groups to avoid any cross-contamination. In addition, the fecal samples were collected by forceps (cleaned with alcohol before each use) to avoid any cross-contamination. Thus, there is little to no possibility of only one group exposing to specific environmental microbes leading to their altered fecal microbiome as observed in our study.

Animal experiments and maintenance were approved by the IACUC of the Rush University Medical Center (Chicago, IL). The study involved a total of 28 mice that were randomized into four groups (n=7 in each): vehicle, rotenone, RS, and RS+rotenone. Mice were acclimated to the facility for two weeks prior to initiation of the study (Week -2 to 0). Mice underwent baseline training and testing for the rotarod for three weeks (Week 0 to 3). Restraint

stress was initiated during week three and continued for the duration of the study. After six weeks of RS, a test for gut permeability was conducted and stool was collected for microbiota analysis. Rotenone (or vehicle) was administered daily from week 9 through week 15 followed by behavioral tests, permeability assay, stool collection, sacrifice and tissue harvest during week 15 (Figure 1A).

Rotenone gavage

For rotenone intoxication, mice received oral gavage of a freshly-prepared (10 minutes prior to gavage) rotenone solution (or vehicle control) at a dose of 10mg/kg/day body weight, suspended in vehicle (4% carboxymethylcellulose and 1.25% chloroform).[27]

Chronic restraint stress (RS) protocol

For RS administration, mice (n=14 total) were kept in 50ml conical tubes for 2 hours/day (5 days/week) throughout the study. RS was performed between 10:00am-3:00pm at different times to minimize acclimation to the daily RS treatment. The tubes had multiple holes (approximately 0.5cm size) to allow airflow and also prevent hyperthermia. Control mice were housed alone in a new cage for two hours without food and water. Fecal pellets for each mouse were collected during these two hours. Immediately after RS, mice were returned to the home cage and had access to food and water *ad libitum*. To confirm the effectiveness of the RS protocol, four parameters were recorded: 1) weekly body weight, 2) weekly 24h food intake (starting at week 7), 3) weekly fecal output (total weight of stool pellets) during RS session, and 4) urinary cortisol was measured after six weeks of chronic RS before rotenone administration.

Behavior studies

Three different behavioral experiments were conducted including: 1) rotarod for motor impairment, 2) adhesive removal test for sensory and motor impairment, and 3) hanging grip test for muscle strength. 1) Rotarod test was performed at three different times (baseline (week 3), week 9, week 15). During this procedure, mice were placed on rod with a speed of 2 rpm and the speed was gradually increased to 90 rpm during the 90s trial. Time to fall was recorded. Three trials were performed for each mouse with a 15 min interval between trials. 2) Adhesive removal test was performed at week 14. During the test procedure, animals were allowed to move freely in a clean cage for one minute prior to the test to allow for acclimation. Stickers were applied to the front paws with gentle pressure and mice were then placed back into the testing cage and time for each animal to remove both stickers was recorded. Three trials were recorded for each mouse with a minimum of a 15 min interval between each trial. 3) Hanging grip test was performed at week 14. During this procedure, mice were kept on a wire mesh for one minute before the test procedure for acclimation. The wire mesh was then inverted and total hang time was recorded for each mouse before they fell into a cage below. Three trials were recorded for each mouse with 15 minute intervals between trials.

Intestinal permeability and markers of microbial translocation (MMT) measurements

Gut permeability was measured using an established protocol[77] at three different times (baseline (week 3), week 9, week 15). In brief, mice were fasted overnight prior to the permeability test to prevent confounding factors associated with dietary sugar intake. During the test, mice were gavaged with a solution of non-absorbable, poorly digestible sugar (sucralose, lactulose, mannitol, sucrose) and given a subcutaneous injection of saline (0.9%) to promote

urine production. Mice were then placed into individual metabolic chambers for five hours to collect urine. Gas chromatography was performed on the urine samples to measure excreted levels of sugars during the five hours. Urinary data were recorded as percentage excretion of oral dosage. Fecal pellets were also collected and stored at -80^{o}C for future analysis. We used sugar cocktail markers to assess intestinal permeability because: (1) unlike other markers such as FITC-Dextran, it provides an opportunity to identify the region of the gut where hyperpermeability primarily occurs. For example, mannitol is primarily absorbed in the proximal small bowel and with a molecular weight of 182 Da is a marker for both pores and leak pathways. Lactulose and sucralose are both larger size molecules and are markers of leak pathway only. Both lactulose and sucralose can be absorbed in both small and large intestine but since lactulose can be fermented by colonic bacteria, it primarily represents small intestinal permeability marker. Thus, if urinary mannitol/lactulose are normal while urinary sucralose is elevated, it represents that disruption of intestinal barrier is primarily through leak pathway and is primarily is in the colon. Furthermore, unlike FITC marker, sugar cocktail can be used to assess intestinal permeability in both rodents and human. Importantly, our hypothesis of stress-induced hyper-permeability and its role in PD pathogenesis was based on our groups' published data that intestinal leak in PD patients is primarily in the colon with significantly elevated urinary sucralose and normal mannitol and lactulose levels [12] and Sucralose/lactulose ratio [28]; (2) unlike FITC marker, sugar cocktail can be used to assess intestinal permeability in both rodents and human.

Levels of markers of microbial translocation (MMT) were measured using plasma samples of the mice collected during sacrifice. Lipopolysaccharides (LPS) (N384, Pyrogent

5000) and LPS binding protein (LBP) (HK205, Hyarlt Biotech) were measured using ELISA kits according to the manufacturer protocol.

Sacrifice and tissue collection

Necropsy was performed under anesthesia as approved by Rush IACUC#14-011. Blood (~500µl) was collected by cardiac puncture and stored on ice to collect plasma. After blood collection, animals were perfused with cold saline. The descending aorta was clamped using hemostatic forceps to perfuse the upper body. Brain and intestinal tissue samples were harvested and stored either in optimal cutting temperature (OCT) media (4583, Tissue-tek), as fresh frozen tissue for proteomic analyses, or in 4% paraformaldehyde (overnight) for histology.

Immunohistochemistry

Brain sections were cut using a microtome at 40 µm thickness and sections were stored in cryoprotectant. Colon samples were cut at 6µm thickness using a cryostat (CM3050, Leica) and were mounted on glass slides for analysis. Histology was performed on paraformaldehyde fixed brain samples using an established method [78] and colon samples according to an established protocol.[37] In brief, sections were washed with phosphate buffer saline (PBS) for 30 minutes. An endogenous sodium peroxidase block was performed using sodium periodate solution for 20 minutes. Following peroxidase blocking, sections were washed multiple times in PBS and incubated in serum blocking solution for an hour (2% BSA and 3% serum targeting host of the secondary antibody). Primary antibodies to ZO-1 (1:200; 617300; Invitrogen), occludin (1:200; 331500; Life technology), claudin-1 (1:200; 717800; Invitrogen), N-tyrosine (1:200, 06-204, Millipore), α-syn (1:200, LB509, Invitrogen), and GFAP (1:500; Z0334, DAKO) were used for

the colon tissue while antibodies to Iba1 (1:500; 019-19741, Wako), TH (1:1000; AB152, Millipore), LPS (1:250; ab35654, Abcam), and TLR4 (1:150; ab13556, Abcam) were used for the brain tissue staining. Sections were kept in the primary antibody solution overnight at room temperature. The next day, sections were washed and processed with secondary antibody. Immunofluorescence staining was performed using specific fluorescence secondary antibodies (1:400; A21202, A31572, A21432; Life Technologies) while immunoperoxidase staining was performed using biotinylated secondary antibodies (1:200; BA1000, BA2000; Vector Laboratories). Immunoperoxidase sections were treated with actin-biotin complex incubation before developing a color reaction in the presence of DAB chromogen and hydrogen peroxide. Counterstaining was performed using DAPI (1:10,000; Invitrogen) for immunofluorescence slides and hematoxylin (SH26-500D, Fisher) for immunoperoxidase stained slides. Dying cells in the SN were stained using Fluorojade-C (FJ-C) marker as per manufacturer protocol. Once completed, immunofluorescence sections were cover-slipped using aquamount (4583, Tissue-Tek) and stored at 4^0C for confocal microscopic analyses. Immunoperoxidase stained sections were processed through different grades of alcohol (0%-99%) and then incubated in xylene for 15 minutes before applying a coverslip using vectastat 60 mounting media (Life technology).

Western blot analysis

IL1-β (1:5000; ab9722; Abcam) was evaluated using a Western blot. In brief, tissue was homogenized and followed with bicinchoninic acid assay (BCA assay) to measure total protein concentration. Equal amounts of protein were loaded in each lane of the gel (10% separating acrylamide gel) and separated using electrophoresis. Proteins were then transferred to a nitrocellulose membrane and bands were visualized with an Odyssey infrared scanner after

immunolabeling with the respective primary antibodies followed by an infrared specific fluorophore-tagged secondary antibody.

Cytokine antibody array

Mouse Cytokine Antibody Array C1 was utilized to detect cytokines/chemokines level (AAM-CYT-1-8, RayBiotech, GA) as per manufacturer's protocol. In brief, colon tissue samples were homogenized in a cell lysis buffer (+protease inhibitor) provided by the manufacturer. BCA assay was performed to measure total protein concentration. N=3/4 cases in equal protein concentrations were pooled to run two blots per group. Total of 300µg of protein was incubated onto each membrane for an overnight at 4^{o}C after blocking the membrane with the blocking buffer. Next day, membranes were washed and incubated for biotinylated antibody cocktail (1.5 hours), followed by washes and HRP-streptavidin incubation (2 hours). Chemiluminescence was detected and scanned to perform densitometric analysis using ImageJ. Background was subtracted and data were normalized per blot using positive controls to generate the relative density reads. These data then transformed into Log2 and analyzed using Two-way ANOVA. Heatmap was generated using R software for the Log2 data.

Microscopic analysis – cell counts

TH+ cells were evaluated in the left hemisphere of the SN using stereo-investigator software (MBF Bioscience).[78] In brief, level-matched SN sections (n=5) were selected per case to perform the stereology. For each section, the SN was outlined under low magnification (4X). Using grid size (175µmx175µm) and frame size (80µmx80µm), sections were evaluated under high magnification (60X). The estimated number of cells and total estimated volume were

recorded from the Stereology software. Data were reported as estimated neuronal density (estimated number of cells in total volume of outlined SN = cells/mm^3).

Iba1+ microglial cells in the SN were analyzed using Image-J software (Image J 3.1, NIH) blinded. Level-matched SN sections (n=3) were selected to evaluate the Iba1+ microglial cells. Using light microscope (BX61, Olympus), five images per section were taken randomly focusing on the SN region under 60x1.6 magnification. In each image, 16,925μm^2 area was evaluated for Iba1+ cells. Images were processed and uploaded in Image-J and Iba1+ cells were counted according to their morphology characteristics. Cell morphology was assessed using three different phenotypes as published:[5, 79-81] 1) resting (normal ramification and smaller cell body), 2) activated (higher ramification and larger cell body) and 3) dystrophic/phagocytic (two or less processes with larger cell body, amoeboid shape).

Microscopic analysis - Optical Density (OD) measurements

Image J software was used to measure the intensity of N-tyrosine expression in the lamina propria, GFAP+ enteric glial cells expression in the lamina propria, GFAP+ enteric glial cells in the myenteric plexuses, and α-syn expression in the myenteric plexuses of the colon samples. Fluorescence images were captured using a confocal microscope under higher magnification. Images were processed for compatibility with Image J software and regions of interest were selected to measure the intensity. Background was measured and subtracted from the measured readings. Data were recorded as mean intensity measures.

Microscopic analysis – Integrity score measurements for tight junction proteins

Quantification of the tight junction barrier integrity was performed as published [37] using scale (0 – 3) for tight junction protein immunofluorescence sections (0 = no immunofluorescence, 1 = very light and discontinuous immunofluorescence, 2 = intense and discontinuous immunofluorescence, 3 = smooth continuous and well organized immunofluorescence). Two sections were used for imaging analyses. The slides were randomized and coded to collect fluorescence images to avoid bias. A minimum of twenty crypts were analyzed and the average values were collected for analysis.

HPLC measurements for DA and its metabolites

Striatal DA, DOPAC, and HVA were quantified previously described [82, 83]. Briefly, striatum from half of the brain was collected and immediately frozen using dry ice and stored at -80˚C until the analysis. During HPLC measurements, striatal tissues were sonicated in perchloric acid (0.2M) containing isoproterenol and left on ice for 20 minutes. The resulting homogenates were centrifuged at 10,000g for 15min at 4˚C. After centrifugation, 10µl of supernatant was injected onto an Eicompak SC-3ODS column (HPLC-ECD System, JM Science, EiCOMHTEC-500) and analyzed per manufacture protocol. Standard peaks were generated using 10µg of DA, DOPAC, and HVA to calculate the concentrations in each sample. Data were presented in ng/kg of tissue.

Microbiota sequencing using 16S-rDNA technique

Total DNA was extracted from mice feces utilizing FastDNA bead-beating Spin Kit for Soil (MP Biomedicals, Solon, OH) and processed using high-throughput Illumina amplicon sequencing at Argonne National Laboratory, as described previously.[37] Raw FASTQ files for

each sample were merged using the software package PEAR (Pair-end-read merger) (V0.9.8).[84] Merged reads were quality trimmed and sequences shorter than 250 bases were discarded (CLC genomics workbench (V10.0, CLC Bio, Qiagen, Boston, MA). Sequence data were screened for chimeras, rarefied (25,000), and operational taxonomic units (OTU) classified, as described previously.[37] A biological observation matrix (BIOM) [85] was generated at taxonomic level from phylum to genus ("make OTU table" algorithm) and analyzed using software packages Primer7 [86] and the *R* programming environment.[87]

Alpha diversity indices and Beta diversity were used to examine changes in microbial community structure between mice fecal group samples. To study differences in overall microbial community composition between fecal samples, pairwise Bray-Curtis dissimilarity (non-phylogenetic) metrix was generated using Primer7 software package and used to implement analysis of similarity (ANOSIM) calculations. ANOSIM was performed at the taxonomic levels of phylum, family, and genus, using square-root transformed data.

Within the software package QIIME [88], differences in relative abundances of individual taxa, between defined groups, were analyzed for significance using Kruskal-Wallis test, generating both *P*-value and a Benjamini-Hochberg false-discovery rate (FDR) corrected *P*-value. Significant taxa differences were reported at FDR-$P<0.05$ or taxa relevant to this study, with $P<0.05$ values. Furthermore, mice fecal group sample's community functional predictions were performed using PICRUSt (Phylogenetic Investigation of Communities by Reconstruction of Unobserved States) [89] and differences in Kyoto Encyclopedia of Genes and Genomes (KEGG) ortholog (KO) abundances between groups were identified.[90]

The raw sequence data (FASTQ files) were deposited in the National Center for Biotechnology Information (NCBI) Sequence Read Archive (SRA), under the BioProject identifier PRJNA454894.

Fecal short chain fatty acid measures

SCFAs were extracted and quantified by GC-MS for stool samples from 28 mice. Absolute quantities of acetic, propionic, isobutyric, butyric, isovaleric, and valeric acids were determined by using spiked heavy labelled internal standards. Briefly, 80 mg frozen pellet, 0.5 mL of cold 0.1 M HCl containing 200 µg/mL of 13C2-acetic acid and 10 µg/mL of 13C4 sodium butyrate were added. Samples were vigorously shaken on a vortex plate for 15 min and then sonicated for 10 min in cold water bath. Then the samples were centrifuged at 15,000 *g* for 15 min at 4°C. Supernatants (250 µL) were recovered, and added to 0.5 mL MTBE, followed by vortexing for 10 s. The top MTBE layer was recovered after centrifugation at 2,000 rpm for 2 min, and stored at 4°C until analysis. The MTBE extract (1 µL) of SCFAs were injected into a Trace 1310 GC coupled to a Thermo ISQ-LT MS, at a 5:1 split ratio. The inlet was held at 240°C and transfer line was held at 240°C. SCFA separation was achieved on a 30m DB-WAXUI column (J&W, 0.25 mm ID, 0.25 µm film thickness). Oven temperature was held at 80°C for 0.5 min, ramped at 10°C/min to 175°C, then ramped to 240°C at 40°C/min, and held at 240°C for 3 min. Helium carrier gas flow was held at 1.2 mL/min. SIM mode was used to scan ions 45, 60, 62, 73, 74, 76, 87, 88, 92 at a rate of 10 scans/sec under electron impact mode. Acetic, propionic, isobutyric acids were quantified by IS - 13C2-acetic acid. Butyric, isovaleric, and valeric acids were quantified by IS - 13C4 sodium butyrate.

Rotenone measurements in the brain and liver

Brain rotenone levels were measured at Mass Spectrometry, Metabolomics and Proteomics Facility at the UIC. In brief, rotenone was dissolved in MS grade H2O: Acetonitrile (1:4, v:v). A standard curve was created with 7 points: 200fg, 500fg, 1pg, 5pg, 15pg, 50pg and 100pg. Brain samples were stored at -80^{o}C until use. Brain was placed into a bead-beating tube and 400µL of acetonitrile was added and tissue beat for 2x10 seconds. Samples were centrifuged at 14000g at 4^{o}C for 10min and 200µL of supernatant were collected. Samples were dried with N2 and reconstituted with 100µL H_2O: Acetonitrile (1:4, v:v).The LC/MS analysis was performed on AB Sciex Qtrap 5500 MS coupled to Agilent 1290 UPLC system. All samples were analyzed by Phenomenex HPLC C18 Column, 100Å, 2.6 µm, 2.1 mm X 50 mm coupled to an Agilent 1290 UPLC system, which was operated at a flow rate of 400µL/min. A gradient of buffer A (H20, 0.1% Formic acid) and buffer B (Acetonitrile, 0.1% Formic acid) was applied as: 0 min, 1% of buffer B; increase buffer B to 50% in 3 min; 50%-90% in 2 min; Kept B at 100% for 3 min. The column was equilibrated for 2 min at 1% B between the injections. The column temperature was 40^{o}C and the autosampler was kept at 4^{o}C. The MS condition of analytes was optimized on tuning mode; the results are listed in Supplemental Figure 3. The quantification was achieved using area of monitored transitions. All the samples were analyzed by triplicate.

Liver rotenone levels were measured by LC-MS. The service was performed by Dr. Yue-Ting Wang at the Mass Spectrometry Core in Research Resources Center of University of Illinois at Chicago. In brief, Initial solution of rotenone was prepared at 1 mg/ml in acetonitrile (ACN). It was then diluted to 10 µg/ml, 100 ng/ml, 10 ng/ml, 5 ng/ml, 1 ng/ml, 0.2 ng/ml, 0.1 ng/ml, and 0.05 ng/ml as the standard solutions used to prepare the standard curve. All stock solutions were stored at -20C.

The mixture solvent (1.2 mL) with MeOH and water (1:1, v/v) was added to the frozen liver tissues (about 100 mg), which were then homogenized (30 frequency) for 2 min. The suspension was centrifuged at 4°C and 13,500 g for 10 min, and the resulting supernatant (MeOH/water (MW) extracts) was transferred to a 2 ml microcentrifuge tube. The remaining pellets were extracted again with 1 ml of the mixture solvent (dichloromethane:MeOH, 3:1, v/v). The supernatants (dichloromethane/MeOH (DM) extracts) were collected in new microcentrifuge tubes following centrifugation. Each extract solution was evaporated with a speed-vacuum machine. Dried samples were stored at −80°C.To each "MW" sample, 300 µl of ACN was added. To each "DM" sample, 100 µl of ACN was added. Samples were vortexed vigorously, then centrifuged at 15000 rpm for 15 min. 25 µl of supernatant was taken from each sample for LCMS analysis.

Two µL of sample or standard solution was injected into Sciex Qtrap 6500 coupled with Agilent 1290 UPLC system. All samples were eluted by Phenomenex Kinetex C18 column (1.7 µm, 2.1 x 50 mm) kept at 40 degrees at a flow rate of 450 ul/min. LC elution started with 60% mobile phase A (5% ACN in H2O with 0.1% FA) for 1 min, followed by a linear gradient increase of mobile phase B (ACN with 0.1% FA) from 40 to 95% in 2 min. MS data were acquired by MRM scan at positive mode. The ESI spray voltage and source temperature was set at 4.7 kV and 450 degrees. Positively charged rotenone was detected by monitoring its transitions to signature product ions 395>192 and 395>213. The quantification was achieved using the peak area of monitored transition 395>213.

The standard curve of rotenone was plotted with the concentration as X axis and the peak area of the target as Y axis. Six non-zero calibrators were used to construct the standard curve. The curve was fitted by linear regression with a weighting factor of 1/x. The norminal

concentrations, back calculated concentrations and accraucy of calibrators are listed in Table 1. The accuracy of each calibrator is within the acceptable range of 15%. The limit of quantitation (LOQ) is 0.1 ng/ml—with 2 µl injection that results in 200 fg on column. Lower point 0.05 ng/ml (100 fg on column) was detectable but not quantifiable. Good concentration-response linearty (r = 0.9999) was established over the range from 0.1 ng/ml to 100 ng/ml. Quantitation results were generated using Analyst software.

Statistical analyses

All data are reported as mean+standard error of the mean (SEM), unless otherwise stated. Differences among means were analyzed using GraphPad Prism (v5.03) software (GraphPad Software, Chicago, IL). Repeated measures (rm) analysis of variance (ANOVA) was performed to evaluate the time effect on various behavior parameters among groups. Two-tailed unpaired independent t-test was performed to compare two groups. One-way ANOVA was performed to evaluate the significance differences between multiple groups. Two-way ANOVA was performed to evaluate the significant differences with conditions (control vs RS), treatments (vehicle vs rotenone) or an interaction (stress by rotenone). Multiple group comparisons were performed using Bonferroni post-hoc comparisons. The significance was considered at the value $P<0.05$.

Figure legends:

Figure 1: Restraint stress (RS) protocol effectively increased established measures of chronic stress in mice. (A) Mice (n=14) were subjected to unpredictable RS (2h, 5days/week) from week 3 to week 15 (time of sacrifice). Intestinal permeability was measured at baseline (week 1), after six weeks of RS (week 9), followed by six weeks of RS±rotenone treatment (week 15). Graphs in panels represent (B) Body weight (rmANOVA showed significant effect of (group) $F_{(1,24)}$=12.19, P=0.002; (time) $F_{(7,168)}$=12.18, P<0.0001; (interaction) $F_{(7, 168)}$=22.22, P<0.0001), (C) 24h food intake (rmANOVA: $F_{(1,24)}$=2.325, P=0.14), (D) fecal output data during 2h of restraint stress (rmANOVA: (groups) $F_{(1,24)}$=147.3, P<0.0001; (time) $F_{(13, 312)}$=10.82, P<0.0001; (interaction) $F_{(13, 312)}$=5.443, P<0.0001) and (E) urinary cortisol after six weeks of RS (week 9). RS group showed higher urinary cortisol compared to control (two-tailed, unpaired T test: $t_{(12)}$=2.49, P=0.03). Data are mean ± SEM for panels (B, C, and D) and mean+SEM for a panel (E). *P<0.05, **P<0.01, ***P<0.001.

Figure 2: Restraint stress (RS) promoted rotenone-induced intestinal permeability, endotoxemia, and tight junction barrier loss. Mice were subjected to an initial six weeks of unpredictable RS (2h/day, 5days/week) followed by six weeks of RS±Rotenone treatment. Graph in panels represent (A) Percent excretion of sucralose/lactulose after six weeks of RS subtracted from the baseline. RS group showed higher % excretion of sucralose/lactulose compared to control (two-tailed, unpaired T test: $t_{(26)}$=3.14, P<0.00), (B) Percent excretion of sucralose/lactulose after 12 weeks of RS±rotenone subtracted from the baseline (Two-way ANOVA showed significant effect of stress ($F_{(1,22)}$=11.91, P<0.00) and no significant effects of rotenone nor an interaction), (C) Plasma levels of LPS endotoxin (Two-way ANOVA showed significant effect of stress ($F_{(1, 22)}$=4.33, P<0.05) and no significant effect of rotenone nor an

interaction), and (D) plasma levels of LBP (Two-way ANOVA showed significant effect of rotenone ($F_{(1, 22)}$=7.14, *P*=0.01) and no effect of stress nor an interaction). (E) Representative immunofluorescence images for the tight junction proteins ZO-1, occludin, and claudin 1 in the colon tissue. Arbitrary scale of 0-3 scores (0=no expression - 3=continuous normal expression of the barrier) was used to score barrier integrity. Graphs in panels represent (F) Integrity scoring data for ZO-1 (Two-way ANOVA showed significant effect of stress ($F_{(1, 22)}$=12.57, *P*<0.00) and no effect of rotenone nor an interaction), (G) integrity scoring data for occludin (Two-way ANOVA showed significant effect of stress ($F_{(1, 22)}$=39.38, *P*<0.00) and no effect of rotenone nor an interaction), and (H) Integrity scoring data for claudin 1 (Two-way ANOVA showed significant effect of stress ($F_{(1,22)}$=5.71, *P*=0.03) and rotenone ($F_{(1,22)}$=4.56, *P*=0.04) but no significant stress and rotenone interaction). Data are mean + SEM; **P*<0.05, ***P*<0.01, ****P*<0.001; n=14 mice in panel (A) and n=7 mice/group (except RS+rotenone group (n=5)) for all other panels (B-H). RS=restraint stress, LPS=Lipopolysaccharides, LBP=LPS binding protein, ZO-1=Zonula occludens-1. Scale bar in E represents 50µm and applies to all panels in E.

Figure 3: Restraint stress (RS) and rotenone showed distinct changes in fecal microbiota and Short Chain Fatty Acid (SCFA) levels. (A) Stacked histograms depicting 90% of the rarefied sequences of microbial taxa (relative abundance of total bacteria at family) between mice fecal groups: No changes at baseline; significant differences observed at both week 9 and 15 between groups. (B) The relative abundance of genus *Lactobacillus,* specifically at week 9, indicated a significant decrease in RS mice compared to control mice. (C) The relative abundance of (detectable gram-negative) genera *Desulfovibrio, Bacteroides, and Akkermansia* at all three timepoints. Two-Way ANOVA indicated *Akkermansia* was significantly impacted by rotenone ($F_{(1,24)}$=9.78, *P*<0.00) and stress ($F_{(1,24)}$=5.18, *P*=0.03). At week 15, post-hoc analysis

showed significantly higher relative abundance of g_*Akkermansia* in RS+rotenone group compared to RS ($p<0.05$). (D) Two-Way ANOVA indicated stress showed significant effect on the F/B ratio ($F_{(1, 24)} = 4.322$, $P=0.048$) at week 15. Fecal SCFAs measurement using gas chromatography are shown in (E) Butyrate, (F) Acetate and (G) Propionate at week 15. (E) Two-Way ANOVA indicated significant effect of stress on butyrate levels in the feces ($F_{(1, 21)} = 5.706$, $P=0.0264$). Data are mean+SEM; *$p<0.05$, **$p<0.01$, ***$p<0.001$; n=14/group for baseline (week 1) and post-6 weeks RS (week 9) while n=7 mice/group (except RS+rotenone group (n=5)) after RS±rotenone treatment (week 15). RS=restraint stress.

Figure 4: Restraint Stress (RS) increased colonic inflammation markers and rotenone-induced A-SYN pathology. Photomicrographs represent (A) Haematoxylin and Eosin (H & E) and (B) n-tyrosine expression in the lamina propria. Graphs (C) and (D) show optical density analysis of n-tyrosine reactivity (Two-way ANOVA showed significant effect of stress and rotenone interaction ($F_{(1,20)}=6.25$, $P=0.02$) but no significant effect of stress or rotenone only) and cell count analysis of n-tyrosine positive cells (two-way ANOVA showed significant effect of stress ($F_{(1,20)}=10.69$, $P<0.00$) but no significant effect of rotenone or interaction) in the lamina propria. (E) Pro-inflammatory cytokine IL1β expression using western blot analysis. Two-way ANOVA showed significant effect of stress ($F_{(1,22)}=9.08$, $P=0.01$) but no effects of rotenone or interaction. (F) Representative images of enteric glial cells (GFAP+) expression and alpha-synuclein (A-SYN) expression in the myenteric plexuses. Graphs (G, H) show optical density analysis of GFAP expression in the lamina propria (Two-way ANOVA showed significant effect of stress and rotenone interaction ($F_{(1,22)}=5.43$, $P=0.03$) but no significant effect of stress or rotenone alone) and myenteric plexuses (Two-way ANOVA showed significant effect of stress ($F_{(1,22)}=17.49$, $P<0.00$) and rotenone ($F_{(1,22)}=53.49$, $P<0.00$) but not significant interaction).

Graph (I) represent optical density analysis for a-syn expression in the myenteric plexuses (Two-way ANOVA showed significant effect of rotenone ($F_{(1,22)}$=21.17, P<0.00) but no significant stress effect or stress and rotenone interaction). Data are mean + SEM; *p<0.05, **p<0.01, ***p<0.001; n=7 mice/group (except RS+rotenone group (n=5)) for all panels. Scale bar in B and F represents 50µm and applies to all panels in B and F. RS=restraint stress, OD = optical density, GFAP = Glial fibrillary acidic protein, A-SYN = alpha-synuclein.

Figure 5: Restraint stress (RS) in combination with rotenone potentiated neuro-inflammation and degeneration. (A) Representative pictures of Iba1+ microglia cells in the SN. (B) Representative images of resting microglia, activated microglia and dystrophic/phagocytic microglia, (C) graph shows estimated Iba1+ cells in the SN based on their morphology characteristics. Two-way ANOVA showed significant differences in microglia morphology between groups. (D) Representative immunofluorescence images of FJ-C+ dying cells in combination with TH+ dopamice cells in the SN. (E) Representative images of LPS reactivity in the SN. (F) Representative images of TH+ dopamine cells in the SN and (G) stereological estimates (two-way ANOVA showed significant effect of rotenone ($F_{(1,22)}$=49.63, P<0.00) but no significant stress effect or interaction). (H, I, J) HPLC measured levels of dopamine and dopamine metabolites in the striatum. Two-way ANOVA showed that striatal dopamine levels were significantly affected by rotenone ($F_{(1,22)}$=10.52, P<0.00), stress ($F_{(1,22)}$=8.48, P=0.01), as well as a rotenone by stress interaction ($F_{(1,22)}$=8.57, P=0.01) while DOPAC level showed no significant changes and HVA levels were significantly impacted by stress ($F_{(1,22)}$=12.46, P=0.00) but no significant effect of rotenone or interaction. Data represent mean+SEM; *p<0.05, **p<0.01, ***p<0.001; n=7 mice/group (except RS+rotenone group

(n=5)) for all panels. RS=restraint stress, FJ-C=Fluorojade-C, LPS= lipopolysaccharides, TH=Tyrosine hydroxylase, DOPAC=Dopamine carboxylase, HVA=homovanillic acid.

Figure 6: Restraint stress (RS) in combination with rotenone promotes behavioral deficits. (A) Rotarod behavior at baseline, after six weeks of RS (week 9), and followed by six weeks of RS±rotenone (week 15) (rmANOVA showed significant time and treatment interaction ($F_{(6,44)}$=2.65, P=0.03)). (B) Adhesive removal test at week 14 (Two-way ANOVA showed significant effect of stress ($F_{(1,22)}$=28.59, P<0.00), rotenone ($F_{(1,22)}$=50.63, P<0.00) and stress and rotenone interaction ($F_{(1,22)}$=18.93, P<0.00)). (C) Hanging grip test at week 14 (Two-way ANOVA showed significant effect of rotenone ($F_{(1,22)}$=14.39, P<0.00) and no effect of stress nor an interaction). The data are presented as mean+SEM. *P<0.05, **P<0.01, ***P<0.001. n=7 mice/group (except RS+rotenone group (n=5) at week 15) for all panels. RS=restraint stress.

Figure 7: Pearson correlations support the possible gut-brain axis involvement in leaky gut-induced exacerbated PD phenotype in a rotenone PD mice model. (A) ZO-1 integrity score was significantly inversely correlated with dystrophic/phagocytic microglia counts in the SN. (B) Plasma LPS levels and (C) bacterial taxa *Akkermansia* (mucin degrading gram- bacteria) were significantly positively correlated with dystrophic/phagocytic microglial counts in the SN. (D) Relative abundance of *Akkermansia* (mucin degrading gram- bacteria) were significantly inversely correlated with hanging grip test behavior data. (E) Fecal butyrate levels were significantly positively correlated with striatal DA concentrations.

Supplemental Figure legends:

Figure S1: Restraint stress (RS) did not affect urinary sucrose or mannitol levels. Graphs (n=7, except RS+rotenone: n=5) in panels represent: Percent excretion of sucrose (A) after six weeks of RS and (B) after 12 weeks of RS+rotenone subtracted from the baseline. Similarly, graphs (n=7, except RS+rotenone: n=5) in panels represent: Percent excretion of mannitol (C) after six weeks of RS and (D) after 12 weeks of RS+rotenone subtracted from the baseline. Western blot analyses (n=3/4) were performed on tight junction proteins (E) Occludin and (F) Claudin 1 from the whole colonic tissue lysate.

Figure S2: Chronic stress and rotenone showed distinct effects on the microbiome at the Phylum taxonomy level. Graphs in panel represent phylum taxonomy at the baseline (A), after six weeks of RS (week 9) (B) and followed by six weeks of RS±rotenone (week 15) (C). Graphs in panel (D) represent alpha diversity indices: Shannon index, Simpson index, Richness and Evenness at the phylum taxonomy. Two-way ANOVA showed significant effect of rotenone with Shannon ($F_{(1,24)}$=8.47, P=0.08), Simpson ($F_{(1, 24)}$=8.77, P=0.01) and Evenness ($F_{(1, 24)}$=7.92, P=0.01) indices at the Phylum level but there were no significant effects of stress or rotenone and stress interaction. The data in (D) are presented as mean+SEM. *p<0.05, **p<0.01, ***p<0.001. n=14 mice/group for baseline and week 9, n=7 mice/group (except RS+rotenone group (n=5)) for week 15. RS=restraint stress.

Figure S3: Rotenone was not in a detectable range in the brain with employed low-dose rotenone protocol (10mg/kg body weight – oral gavage every day for six weeks). Levels of rotenone were measured using HPLC-MS at the time of sacrifice (week 15) in combined olfactory bulb, cortex and rostral striatum brain tissue. Data in panels represent (A) rotenone standard curve, (B) HPLC-MS method strategy, (C) spectrum of original compound using 200fg

rotenone pure sample, (D) spectrum of rotenone spiked brain sample, (E) spectrum of saline (vehicle) spiked brain sample, (F) representative spectrum of rotenone treated mice, (G) representative spectrum of stress+rotenone treated mice. n=7 animals/group.

Figure S4: Restraint stress (RS) altered colonic tissue cytokines. Photomicrographs show (A) representative array blots from each group. Pooled samples of (n=3/4 mice) were employed with the immunoblot-based array to detect the inflammatory mediators (n=2 blots/group). (B) Log2 normalized densitometric reads were plotted to generate the heat map expression of inflammatory mediator from all blots and two-way ANOVA was performed to find the significant differences among groups. Specifically, IL-9 (P=0.038) and IFN-gamma (P=0.033) levels showed statistically higher levels in RS group compared to control (stress: $F(1, 4)=15.24$, $P=0.0175$, stress by rotenone interaction: $F(1,4)=17.92$, $P=0.013$ respectively). Panel (C) represents the antibody array layout. * $p<0.05$ (Bonferroni post-hoc comparisons)

Figure S5: Lipopolysaccharide (LPS) immunohistochemistry in SN from all mice (n=26). Photomicrographs in each panel represent LPS reactivity in the SN of each mice from the Control (n=7), Rotenone (n=7), RS (n=7) and RS+rotenone (n=5) groups. Overall RS and RS+rotenone showed higher immunoreactivity compared to controls.

Figure S6: Toll-like receptor-4 (TLR4) and Tyrosine Hydroxylase (TH) immune-reactivity in the striatum. Photomicrographs shows representative images of (A) Toll-like receptor-4 (TLR4) immunofluorescence staining and (B) Tyrosine hydroxide immunoperoxidase staining. TLR4 showed no reactivity in the striatum of control but higher reactivity in the striatum of RS and RS+rotenone groups. TH showed reduced expression in RS+rotenone group compared to rotenone. Scale bar in TLR4 panel represents 20µm and TH panel represents 500µm applies to all panels respectively.

Table 1. Alpha diversity at Phylum, Family and Genus taxonomic levels

Time points	Groups				Taxonomy	Diversity Indices	Mean ± SEM				*P* value		
							Control	Rotenone	RS	RS + rotenone	UT-test	ANOVA	Post-Hoc
Baseline													
		Control #	RS #		Phylum	Shannon	0.81±0.02		0.89±0.02		**0.00***		
		Control #	RS #		Phylum	Simpson	0.51±0.01		0.53±0.008		**0.02***		
		Control #	RS #		Phylum	Richness	6.71±0.24		6.92±0.16		0.47		
		Control #	RS #		Phylum	Evenness	0.43±0.01		0.47±0.009		**0.03***		
		Control #	RS #		Family	Shannon	1.44±0.032		1.52±0.038		0.10		
		Control #	RS #		Family	Simpson	0.66±0.009		0.69±0.011		0.09		
		Control #	RS #		Family	Richness	27±0.877		25±0.297		**0.04***		
		Control #	RS #		Family	Evenness	0.44±0.011		0.47±0.012		**0.03***		
		Control #	RS #		Genus	Shannon	1.54±0.038		1.64±0.047		0.12		
		Control #	RS #		Genus	Simpson	0.67±0.009		0.69±0.012		0.09		
		Control #	RS #		Genus	Richness	40.14±1.15		39.29±0.57		0.51		
		Control #	RS #		Genus	Evenness	0.42±0.011		0.45±0.012		0.09		
Post 6 weeks of restraint stress (RS)													
		Control #	RS #		Phylum	Shannon	0.79±0.056		0.83±0.035		0.51		
		Control #	RS #		Phylum	Simpson	0.44±032		0.47±0.024		0.54		
		Control #	RS #		Phylum	Richness	6.54±0.14		6.50±0.138		0.85		
		Control #	RS #		Phylum	Evenness	0.42±0.029		0.45±0.021		0.46		
		Control #	RS #		Family	Shannon	1.32±0.057		1.46±0.062		0.13		
		Control #	RS #		Family	Simpson	0.61±0.026		0.67±0.029		0.18		
		Control #	RS #		Family	Richness	23.3±0.796		24.6±0.693		0.24		
		Control #	RS #		Family	Evenness	0.42±0.017		0.45±0.017		0.21		
		Control #	RS #		Genus	Shannon	1.43±0.059		1.62±0.080		0.08		
		Control #	RS #		Genus	Simpson	0.62±0.027		0.68±0.031		0.16		
		Control #	RS #		Genus	Richness	37.00±0.919		37.93±0.835		0.46		

		Control #	RS #		Genus	Evenness	0.39±0.015		0.44±0.020		0.07		
Post 12 weeks of restraint stress (RS) ± Rotenone													
	Control !	RS !	Rotenone !	RS + Rotenone !	Phylum	Shannon	1.03±0.074	1.11±0.019	**0.89±0.052**	**1.11±0.044**		**0.02 ***	**<0.05**
	Control !	RS !	Rotenone !	RS + Rotenone !	Phylum	Simpson	0.58±0.41	0.63±0.012	**0.54±0.018**	**0.64±0.017**		**0.03 ***	**<0.05**
	Control !	RS !	Rotenone !	RS + Rotenone !	Phylum	Richness	7.00±0.22	7.00±0.22	7.00±0.00	7.00±0.00		1.00	
	Control !	RS !	Rotenone !	RS + Rotenone !	Phylum	Evenness	0.53±0.038	0.57±0.017	**0.46±0.026**	**0.57±0.023**		**0.02 ***	**<0.05**
	Control !	RS !	Rotenone !	RS + Rotenone !	Family	Shannon	1.77±0.059	1.66±0.063	1.69±0.030	1.73±0.052		0.47	
	Control !	RS !	Rotenone !	RS + Rotenone !	Family	Simpson	0.75±0.020	0.73±0.016	0.75±0.008	0.76±0.016		0.72	
	Control !	RS !	Rotenone !	RS + Rotenone !	Family	Richness	27.3±0.714	26.7±0.892	29.9±1.079	27.4±1.192		0.14	
	Control !	RS !	Rotenone !	RS + Rotenone !	Family	Evenness	0.54±0.015	0.50±0.017	0.50±0.008	0.52±0.012		0.20	
	Control !	RS !	Rotenone !	RS + Rotenone !	Genus	Shannon	1.867±0.0711	1.764±0.073	1.823±0.039	1.83±0.065		0.72	
	Control !	RS !	Rotenone !	RS + Rotenone !	Genus	Simpson	0.75±0.021	0.74±0.018	0.76±0.009	0.76±0.017		0.85	
	Control !	RS !	Rotenone !	RS + Rotenone !	Genus	Richness	41.29±1.04	39.71±1.874	43.43±0.751	40.43±1.49		0.27	
	Control !	RS !	Rotenone !	RS + Rotenone !	Genus	Evenness	0.50±0.015	0.48±0.017	0.48±0.010	0.49±0.016		0.69	

represents n=14 mice, ! represents n=7 mice, UT-test = Unpaired T test, ANOVA = One way ANOVA followed by Tukey post-hoc comparisons.

Table 2. Relative abundance of sequences derived from individual taxa post-6weeks of Restraint stress (RS)

OTU	P	FDR_P	# Seqs	
			Control (n=14)	RS (n=14)
Phylum				
Actinobacteria	0.34	0.68	624.00	808.50
Firmicutes	0.47	0.68	17195.38	16403.14
Bacteroidetes	0.50	0.68	5701.23	6657.14
Proteobacteria	0.56	0.68	385.92	452.57
Verrucomicrobia	0.68	0.68	1044.92	471.86
Family				
Lactobacillaceae	**0.04**	0.29	75.62	25.29
Lachnospiraceae	0.08	0.29	672.15	1188.36
Erysipelotrichaceae	0.11	0.29	13465.54	11012.14
Ruminococcaceae	0.19	0.30	1053.38	1693.93
Coriobacteriaceae	0.41	0.50	626.08	812.71
S24-7	0.44	0.50	5660.77	6642.36
Verrucomicrobiaceae	0.84	0.84	1057.15	473.43
Genus				
f_Lachnospiraceae;g_	**0.00**	**0.02**	339.23	708.50
f_Lactobacillaceae;g__Lactobacillus	**0.03**	0.14	73.92	24.93
f_Erysipelotrichaceae;g__Allobaculum	0.10	0.24	13320.31	10771.29
f_Ruminococcaceae;g_	0.11	0.24	626.77	977.21
f_Ruminococcaceae;g_Oscillospira	0.13	0.24	283.00	568.93
f_S24-7;g_	0.50	0.59	5666.85	6667.36
f_Coriobacteriaceae;g_	0.53	0.59	531.15	697.36
f_Verrucomicrobiaceae;g_Akkermansia	0.84	0.84	1044.92	470.50

OTU= Operational Taxonomic Units, g_=unknown genus, RS=restraint stress, # Seqs = average number of sequences in defined group. P-valuea & FDR-Pb = $P < 0.05$: Kruskal-Wallis one-way ANOVA non-parametric multiple comparison test.

Table 3. Relative abundance of sequences derived from individual taxa after 12 weeks of RS ± rotenone.

Taxonomic Level	Feces: Control vs Rotenone				Feces: Control vs RS				Feces: RS vs RS + rotenone			
	# Seqs Control	# Seqs Rotenone	*P*-Value[a]	FDR-*P*[b]	# Seqs Control	# Seqs RS	*P*-Value[a]	FDR-*P*[b]	# Seqs RS	# Seqs RS+Rotenone	*P*-Value[a]	FDR-*P*[b]
Phylum												
Actinobacteria	260.86	98	**0.04***	0.18	260.86	143	0.31	0.38	143	85.14	**0.01***	**0.02***
Verrucomicrobia	3477.14	5998.29	0.14	0.35	3477.14	946.43	0.06	0.28	946.43	4268.43	**0.03***	**0.04***
Firmicutes	12914.57	10844.57	0.48	0.8	12914.57	13586.57	0.41	0.41	13586.57	9798.86	**0***	**0.01***
Bacteroidetes	7807.43	7489	0.65	0.82	7807.43	9795.43	0.11	0.28	9795.43	10328.86	0.65	0.82
Proteobacteria	475	526.29	0.95	0.95	475	372.43	0.2	0.37	372.43	372.86	0.95	0.95
Family												
Coriobacteriaceae	214.86	92.57	0.08	0.57	214.86	134.57	0.9	0.9	134.57	72.71	**0***	**0.03***
Verrucomicrobiaceae	3460.29	6015.14	0.14	0.57	3460.29	928.29	0.08	0.22	928.29	4253.43	**0.03***	0.1
Erysipelotrichaceae	7714.14	5455	0.22	0.6	7714.14	6164.14	0.57	0.65	6164.14	3735.43	0.08	0.17
Ruminococcaceae	1350.71	1389.57	0.41	0.81	1350.71	1905.57	0.14	0.23	1905.57	1743.57	0.75	0.75
Lachnospiraceae	738.29	687.57	0.57	0.9	738.29	797.57	0.57	0.65	797.57	1045.43	0.48	0.64
S24-7	6562.57	7126.14	0.75	0.95	6562.57	8889.57	0.11	0.22	8889.57	9662.71	0.48	0.64
c__Clostridia;o__Clostridiales;f__	2659.57	2957	0.85	0.95	2659.57	4475.29	**0.03***	0.2	4475.29	3031.71	**0.048***	0.13
Lactobacillaceae	236.86	210.57	0.95	0.95	236.86	52.29	0.11	0.22	52.29	157.43	0.65	0.75
Genus												
Akkermansia	3463.14	6033.29	0.14	0.85	3463.14	954.14	0.08	0.17	954.14	4298.71	**0.03***	0.21
Allobaculum	7659.86	5350.29	0.22	0.85	7659.86	6019.57	0.57	0.57	6019.57	3652.57	0.11	0.32
f__Coriobacteriaceae;g__	126	3.14	0.37	0.85	126	14.14	0.14	0.18	14.14	14	0.34	0.6
f__Ruminococcaceae;g__	760.71	726.14	0.41	0.85	760.71	1114.86	0.06	0.17	1114.86	1010	0.75	0.75
f__Lachnospiraceae;g__	461	400	0.48	0.85	461	388.29	0.28	0.31	388.29	803.71	0.14	0.32
Oscillospira	414.14	494.14	0.57	0.85	414.14	604.29	0.06	0.17	604.29	618.71	0.75	0.75
f__S24-7;g__	6561.86	7105.43	0.75	0.95	6561.86	8922.29	0.11	0.17	8922.29	9631.57	0.48	0.72

o__Clostridiales;f__;g__	2657	2960.71	0.85	0.95	2657	4480.57	**0.03***	0.17	4480.57	3037.14	**0.048***	0.21
Lactobacillus	234.57	216.57	0.95	0.95	234.57	53.14	0.11	0.17	53.14	152	0.75	0.75

References:

1. Bartels AL, Leenders KL. Neuroinflammation in the pathophysiology of Parkinson's disease: evidence from animal models to human in vivo studies with [11C]-PK11195 PET. Mov Disord 2007;22(13):1852-1856.
2. Block ML, Hong JS. Microglia and inflammation-mediated neurodegeneration: multiple triggers with a common mechanism. Prog Neurobiol 2005;76(2):77-98.
3. Hirsch EC, Hunot S. Neuroinflammation in Parkinson's disease: a target for neuroprotection? Lancet Neurol 2009;8(4):382-397.
4. McGeer PL, McGeer EG. Inflammation and neurodegeneration in Parkinson's disease. Parkinsonism Relat Disord 2004;10 Suppl 1:S3-7.
5. Norden DM, Muccigrosso MM, Godbout JP. Microglial priming and enhanced reactivity to secondary insult in aging, and traumatic CNS injury, and neurodegenerative disease. Neuropharmacology 2015;96(Pt A):29-41.
6. Sekiyama K, Sugama S, Fujita M, et al. Neuroinflammation in Parkinson's Disease and Related Disorders: A Lesson from Genetically Manipulated Mouse Models of alpha-Synucleinopathies. Parkinsons Dis 2012;2012(271732):8.
7. Xanthos DN, Sandkuhler J. Neurogenic neuroinflammation: inflammatory CNS reactions in response to neuronal activity. Nat Rev Neurosci 2014;15(1):43-53.
8. Abbott RD, Petrovitch H, White LR, et al. Frequency of bowel movements and the future risk of Parkinson's disease. Neurology 2001;57(3):456-462.
9. Petrovitch H, Abbott RD, Ross GW, et al. Bowel movement frequency in late-life and substantia nigra neuron density at death. Mov Disord 2009;24(3):371-376.
10. Clairembault T, Leclair-Visonneau L, Coron E, et al. Structural alterations of the intestinal epithelial barrier in Parkinson's disease. Acta Neuropathol Commun 2015;3:12.
11. Devos D, Lebouvier T, Lardeux B, et al. Colonic inflammation in Parkinson's disease. Neurobiol Dis 2013;50:42-48.
12. Forsyth CB, Shannon KM, Kordower JH, et al. Increased intestinal permeability correlates with sigmoid mucosa alpha-synuclein staining and endotoxin exposure markers in early Parkinson's disease. PLoS One 2012;6(12):e28032.
13. Scheperjans F, Aho V, Pereira PA, et al. Gut microbiota are related to Parkinson's disease and clinical phenotype. Mov Disord 2015;30(3):350-358.
14. Keshavarzian A, Green SJ, Engen PA, et al. Colonic bacterial composition in Parkinson's disease. Mov Disord 2015;30(10):1351-1360.
15. Zheng G, Wu SP, Hu Y, Smith DE, Wiley JW, Hong S. Corticosterone mediates stress-related increased intestinal permeability in a region-specific manner. Neurogastroenterol Motil 2013;25(2):e127-139.
16. Zheng G, Victor Fon G, Meixner W, et al. Chronic stress and intestinal barrier dysfunction: Glucocorticoid receptor and transcription repressor HES1 regulate tight junction protein Claudin-1 promoter. Sci Rep 2017;7(1):4502.
17. Soderholm JD, Perdue MH. Stress and gastrointestinal tract. II. Stress and intestinal barrier function. Am J Physiol Gastrointest Liver Physiol 2001;280(1):G7-G13.
18. Bailey MT, Coe CL. Maternal separation disrupts the integrity of the intestinal microflora in infant rhesus monkeys. Dev Psychobiol 1999;35(2):146-155.
19. Gareau MG, Silva MA, Perdue MH. Pathophysiological mechanisms of stress-induced intestinal damage. Curr Mol Med 2008;8(4):274-281.

20. Mackos AR, Varaljay VA, Maltz R, Gur TL, Bailey MT. Role of the Intestinal Microbiota in Host Responses to Stressor Exposure. Int Rev Neurobiol 2016;131:1-19.
21. Charcot JM. Lectures on the Diseases of the Nervous System. London: The New Sydenham Society, (English translation by Sigerson G), 1878.
22. Gowers WR. A manual of diseases of the nervous system (American edition). Philadelphia: P. Blakiston, Son & Co., 1988.
23. Charlett A, Dobbs RJ, Purkiss AG, et al. Cortisol is higher in parkinsonism and associated with gait deficit. Acta Neurol Scand 1998;97(2):77-85.
24. Sugama S, Sekiyama K, Kodama T, et al. Chronic restraint stress triggers dopaminergic and noradrenergic neurodegeneration: Possible role of chronic stress in the onset of Parkinson's disease. Brain Behav Immun 2016;51:39-46.
25. Hemmerle AM, Dickerson JW, Herman JP, Seroogy KB. Stress exacerbates experimental Parkinson's disease. Mol Psychiatry 2014;19(6):638-640.
26. de Pablos RM, Herrera AJ, Espinosa-Oliva AM, et al. Chronic stress enhances microglia activation and exacerbates death of nigral dopaminergic neurons under conditions of inflammation. J Neuroinflammation 2014;11:34.
27. Pan-Montojo FJ, Funk RH. Oral administration of rotenone using a gavage and image analysis of alpha-synuclein inclusions in the enteric nervous system. J Vis Exp 2010(44).
28. Shaikh M, Rajan K, Forsyth CB, Voigt RM, Keshavarzian A. Simultaneous gas-chromatographic urinary measurement of sugar probes to assess intestinal permeability: use of time course analysis to optimize its use to assess regional gut permeability. Clin Chim Acta 2015;442:24-32.
29. Shen L, Weber CR, Raleigh DR, Yu D, Turner JR. Tight junction pore and leak pathways: a dynamic duo. Annu Rev Physiol 2011;73:283-309.
30. Furuse M, Itoh M, Hirase T, et al. Direct association of occludin with ZO-1 and its possible involvement in the localization of occludin at tight junctions. J Cell Biol 1994;127(6 Pt 1):1617-1626.
31. Rao RK, Basuroy S, Rao VU, Karnaky KJ, Jr., Gupta A. Tyrosine phosphorylation and dissociation of occludin-ZO-1 and E-cadherin-beta-catenin complexes from the cytoskeleton by oxidative stress. Biochem J 2002;368(Pt 2):471-481.
32. Bruewer M, Luegering A, Kucharzik T, et al. Proinflammatory cytokines disrupt epithelial barrier function by apoptosis-independent mechanisms. J Immunol 2003;171(11):6164-6172.
33. Bruewer M, Utech M, Ivanov AI, Hopkins AM, Parkos CA, Nusrat A. Interferon-gamma induces internalization of epithelial tight junction proteins via a macropinocytosis-like process. FASEB J 2005;19(8):923-933.
34. Seth A, Yan F, Polk DB, Rao RK. Probiotics ameliorate the hydrogen peroxide-induced epithelial barrier disruption by a PKC- and MAP kinase-dependent mechanism. Am J Physiol Gastrointest Liver Physiol 2008;294(4):G1060-1069.
35. Suzuki T, Hara H. Quercetin enhances intestinal barrier function through the assembly of zonula [corrected] occludens-2, occludin, and claudin-1 and the expression of claudin-4 in Caco-2 cells. J Nutr 2009;139(5):965-974.
36. Galley JD, Yu Z, Kumar P, Dowd SE, Lyte M, Bailey MT. The structures of the colonic mucosa-associated and luminal microbial communities are distinct and differentially affected by a prolonged murine stressor. Gut Microbes 2014;5(6):748-760.

37. Engen PA, Dodiya HB, Naqib A, et al. The Potential Role of Gut-Derived Inflammation in Multiple System Atrophy. J Parkinsons Dis 2017.
38. Eckburg PB, Bik EM, Bernstein CN, et al. Diversity of the human intestinal microbial flora. Science 2005;308(5728):1635-1638.
39. Verdam FJ, Fuentes S, de Jonge C, et al. Human intestinal microbiota composition is associated with local and systemic inflammation in obesity. Obesity (Silver Spring) 2013;21(12):E607-615.
40. Mariat D, Firmesse O, Levenez F, et al. The Firmicutes/Bacteroidetes ratio of the human microbiota changes with age. BMC Microbiol 2009;9:123.
41. Hodin CM, Visschers RG, Rensen SS, et al. Total parenteral nutrition induces a shift in the Firmicutes to Bacteroidetes ratio in association with Paneth cell activation in rats. J Nutr 2012;142(12):2141-2147.
42. Peng L, Li ZR, Green RS, Holzman IR, Lin J. Butyrate enhances the intestinal barrier by facilitating tight junction assembly via activation of AMP-activated protein kinase in Caco-2 cell monolayers. J Nutr 2009;139(9):1619-1625.
43. Lewis K, Lutgendorff F, Phan V, Soderholm JD, Sherman PM, McKay DM. Enhanced translocation of bacteria across metabolically stressed epithelia is reduced by butyrate. Inflamm Bowel Dis 2010;16(7):1138-1148.
44. Ploger S, Stumpff F, Penner GB, et al. Microbial butyrate and its role for barrier function in the gastrointestinal tract. Ann N Y Acad Sci 2012;1258:52-59.
45. Zhang J, Song L, Wang Y, et al. Reduction in butyrate-producing Lachnospiraceae contributes to stress-induced visceral hypersensitivity in rats. J Gastroenterol Hepatol 2018.
46. Bush TG, Savidge TC, Freeman TC, et al. Fulminant jejuno-ileitis following ablation of enteric glia in adult transgenic mice. Cell 1998;93(2):189-201.
47. Neunlist M, Van Landeghem L, Mahe MM, Derkinderen P, des Varannes SB, Rolli-Derkinderen M. The digestive neuronal-glial-epithelial unit: a new actor in gut health and disease. Nat Rev Gastroenterol Hepatol 2013;10(2):90-100.
48. Ruhl A, Nasser Y, Sharkey KA. Enteric glia. Neurogastroenterol Motil 2004;16 Suppl 1:44-49.
49. Savidge TC, Newman P, Pothoulakis C, et al. Enteric glia regulate intestinal barrier function and inflammation via release of S-nitrosoglutathione. Gastroenterology 2007;132(4):1344-1358.
50. Kabouridis PS, Lasrado R, McCallum S, et al. Microbiota controls the homeostasis of glial cells in the gut lamina propria. Neuron 2015;85(2):289-295.
51. Maes M, Kubera M, Leunis JC. The gut-brain barrier in major depression: intestinal mucosal dysfunction with an increased translocation of LPS from gram negative enterobacteria (leaky gut) plays a role in the inflammatory pathophysiology of depression. Neuro Endocrinol Lett 2008;29(1):117-124.
52. Lennon EM, Maharshak N, Elloumi H, Borst L, Plevy SE, Moeser AJ. Early life stress triggers persistent colonic barrier dysfunction and exacerbates colitis in adult IL-10-/- mice. Inflamm Bowel Dis 2013;19(4):712-719.
53. Soderholm JD, Yates DA, Gareau MG, Yang PC, MacQueen G, Perdue MH. Neonatal maternal separation predisposes adult rats to colonic barrier dysfunction in response to mild stress. Am J Physiol Gastrointest Liver Physiol 2002;283(6):G1257-1263.

54. Perez-Pardo P, Dodiya HB, Broersen LM, et al. Gut-brain and brain-gut axis in Parkinson's disease models: Effects of a uridine and fish oil diet. Nutr Neurosci 2018;21(6):391-402.
55. Liang S, Wang T, Hu X, et al. Administration of Lactobacillus helveticus NS8 improves behavioral, cognitive, and biochemical aberrations caused by chronic restraint stress. Neuroscience 2015;310:561-577.
56. Bailey MT, Dowd SE, Galley JD, Hufnagle AR, Allen RG, Lyte M. Exposure to a social stressor alters the structure of the intestinal microbiota: implications for stressor-induced immunomodulation. Brain Behav Immun 2011;25(3):397-407.
57. O'Mahony SM, Marchesi JR, Scully P, et al. Early life stress alters behavior, immunity, and microbiota in rats: implications for irritable bowel syndrome and psychiatric illnesses. Biol Psychiatry 2009;65(3):263-267.
58. Qin L, Wu X, Block ML, et al. Systemic LPS causes chronic neuroinflammation and progressive neurodegeneration. Glia 2007;55(5):453-462.
59. Hoban DB, Connaughton E, Connaughton C, et al. Further characterisation of the LPS model of Parkinson's disease: a comparison of intra-nigral and intra-striatal lipopolysaccharide administration on motor function, microgliosis and nigrostriatal neurodegeneration in the rat. Brain Behav Immun 2013;27(1):91-100.
60. Liu M, Bing G. Lipopolysaccharide animal models for Parkinson's disease. Parkinsons Dis 2011;2011:327089.
61. Banks WA, Gray AM, Erickson MA, et al. Lipopolysaccharide-induced blood-brain barrier disruption: roles of cyclooxygenase, oxidative stress, neuroinflammation, and elements of the neurovascular unit. J Neuroinflammation 2015;12:223.
62. Erridge C, Bennett-Guerrero E, Poxton IR. Structure and function of lipopolysaccharides. Microbes Infect 2002;4(8):837-851.
63. Latorre D, Puddu P, Valenti P, Gessani S. Reciprocal interactions between lactoferrin and bacterial endotoxins and their role in the regulation of the immune response. Toxins (Basel) 2010;2(1):54-68.
64. Garate I, Garcia-Bueno B, Madrigal JL, et al. Origin and consequences of brain Toll-like receptor 4 pathway stimulation in an experimental model of depression. J Neuroinflammation 2011;8:151.
65. Garate I, Garcia-Bueno B, Madrigal JL, et al. Stress-induced neuroinflammation: role of the Toll-like receptor-4 pathway. Biol Psychiatry 2013;73(1):32-43.
66. MacDowell KS, Caso JR, Martin-Hernandez D, Madrigal JL, Leza JC, Garcia-Bueno B. Paliperidone prevents brain toll-like receptor 4 pathway activation and neuroinflammation in rat models of acute and chronic restraint stress. Int J Neuropsychopharmacol 2014;18(3).
67. Drouin-Ouellet J, St-Amour I, Saint-Pierre M, et al. Toll-like receptor expression in the blood and brain of patients and a mouse model of Parkinson's disease. Int J Neuropsychopharmacol 2014;18(6).
68. Herrera AJ, Castano A, Venero JL, Cano J, Machado A. The single intranigral injection of LPS as a new model for studying the selective effects of inflammatory reactions on dopaminergic system. Neurobiol Dis 2000;7(4):429-447.
69. Pal GD, Shaikh M, Forsyth CB, Ouyang B, Keshavarzian A, Shannon KM. Abnormal lipopolysaccharide binding protein as marker of gastrointestinal inflammation in Parkinson disease. Front Neurosci 2015;9:306.

70. Wooten GF, Currie LJ, Bovbjerg VE, Lee JK, Patrie J. Are men at greater risk for Parkinson's disease than women? J Neurol Neurosurg Psychiatry 2004;75(4):637-639.
71. Hirsch L, Jette N, Frolkis A, Steeves T, Pringsheim T. The Incidence of Parkinson's Disease: A Systematic Review and Meta-Analysis. Neuroepidemiology 2016;46(4):292-300.
72. Voikar V, Polus A, Vasar E, Rauvala H. Long-term individual housing in C57BL/6J and DBA/2 mice: assessment of behavioral consequences. Genes Brain Behav 2005;4(4):240-252.
73. Martin AL, Brown RE. The lonely mouse: verification of a separation-induced model of depression in female mice. Behav Brain Res 2010;207(1):196-207.
74. Fone KC, Porkess MV. Behavioural and neurochemical effects of post-weaning social isolation in rodents-relevance to developmental neuropsychiatric disorders. Neurosci Biobehav Rev 2008;32(6):1087-1102.
75. Lukkes JL, Mokin MV, Scholl JL, Forster GL. Adult rats exposed to early-life social isolation exhibit increased anxiety and conditioned fear behavior, and altered hormonal stress responses. Horm Behav 2009;55(1):248-256.
76. Ros-Simo C, Valverde O. Early-life social experiences in mice affect emotional behaviour and hypothalamic-pituitary-adrenal axis function. Pharmacol Biochem Behav 2012;102(3):434-441.
77. Summa KC, Voigt RM, Forsyth CB, et al. Disruption of the Circadian Clock in Mice Increases Intestinal Permeability and Promotes Alcohol-Induced Hepatic Pathology and Inflammation. PLoS One 2013;8(6):e67102.
78. Dodiya HB, Bjorklund T, Stansell J, 3rd, Mandel RJ, Kirik D, Kordower JH. Differential transduction following basal ganglia administration of distinct pseudotyped AAV capsid serotypes in nonhuman primates. Mol Ther 2010;18(3):579-587.
79. Kopp BL, Wick D, Herman JP. Differential effects of homotypic vs. heterotypic chronic stress regimens on microglial activation in the prefrontal cortex. Physiol Behav 2013;122:246-252.
80. Streit WJ, Walter SA, Pennell NA. Reactive microgliosis. Prog Neurobiol 1999;57(6):563-581.
81. Wilkinson FL, Sergijenko A, Langford-Smith KJ, Malinowska M, Wynn RF, Bigger BW. Busulfan conditioning enhances engraftment of hematopoietic donor-derived cells in the brain compared with irradiation. Mol Ther 2013;21(4):868-876.
82. Khasnavis S, Roy A, Ghosh S, Watson R, Pahan K. Protection of dopaminergic neurons in a mouse model of Parkinson's disease by a physically-modified saline containing charge-stabilized nanobubbles. J Neuroimmune Pharmacol 2014;9(2):218-232.
83. Rangasamy SB, Dasarathi S, Pahan P, Jana M, Pahan K. Low-Dose Aspirin Upregulates Tyrosine Hydroxylase and Increases Dopamine Production in Dopaminergic Neurons: Implications for Parkinson's Disease. J Neuroimmune Pharmacol 2018.
84. Schmieder R, Edwards R. Quality control and preprocessing of metagenomic datasets. Bioinformatics 2011;27(6):863-864.
85. McDonald D, Clemente JC, Kuczynski J, et al. The Biological Observation Matrix (BIOM) format or: how I learned to stop worrying and love the ome-ome. Gigascience 2012;1(1):7.
86. Clarke KR. Non-parametric multivariate analyses of changes in community structure. Australian Journal of Ecology 1993;18:117-143.
87. Team RDC. R:. A language and environment for statistical computing 2013.

88. Caporaso JG, Kuczynski J, Stombaugh J, et al. QIIME allows analysis of high-throughput community sequencing data. Nat Methods 2010;7(5):335-336.
89. Langille MG, Zaneveld J, Caporaso JG, et al. Predictive functional profiling of microbial communities using 16S rRNA marker gene sequences. Nat Biotechnol 2013;31(9):814-821.
90. Kanehisa M, Goto S. KEGG: kyoto encyclopedia of genes and genomes. Nucleic Acids Res 2000;28(1):27-30.

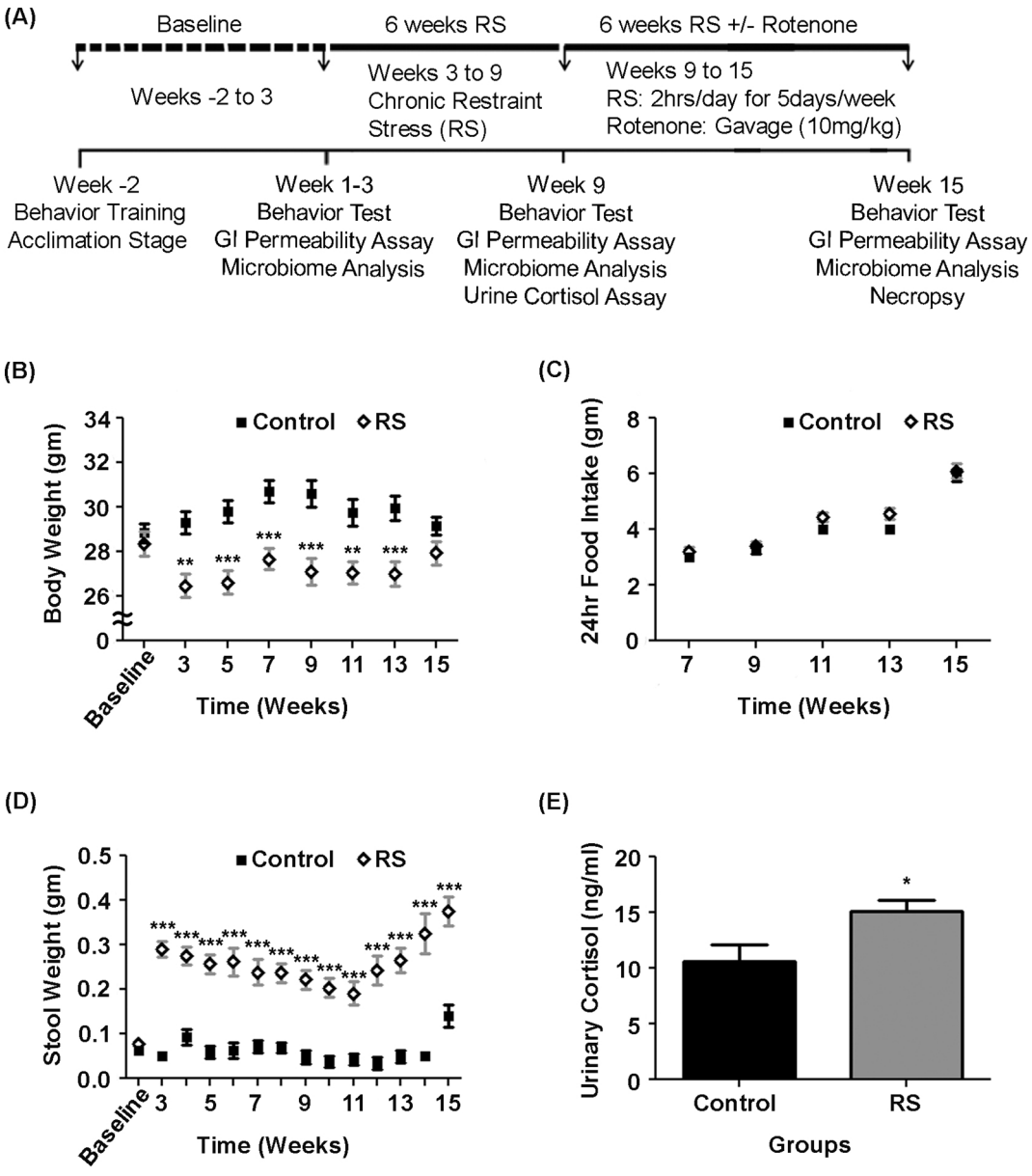
(A)
Baseline
6 weeks RS
6 weeks RS +/- Rotenone
Weeks -2 to 3
Weeks 3 to 9
Chronic Restraint
Stress (RS)
Weeks 9 to 15
RS: 2hrs/day for 5days/week
Rotenone: Gavage (10mg/kg)
Week -2
Behavior Training
Acclimation Stage
Week 1-3
Behavior Test
GI Permeability Assay
Microbiome Analysis
Week 9
Behavior Test
GI Permeability Assay
Microbiome Analysis
Urine Cortisol Assay
Week 15
Behavior Test
GI Permeability Assay
Microbiome Analysis
Necropsy
(B)
Body Weight (gm)
Control
RS
Baseline
Time (Weeks)
(C)
24hr Food Intake (gm)
Control
RS
Time (Weeks)
(D)
Stool Weight (gm)
Control
RS
Baseline
Time (Weeks)
(E)
Urinary Cortisol (ng/ml)
Control
RS
Groups

Figure 1

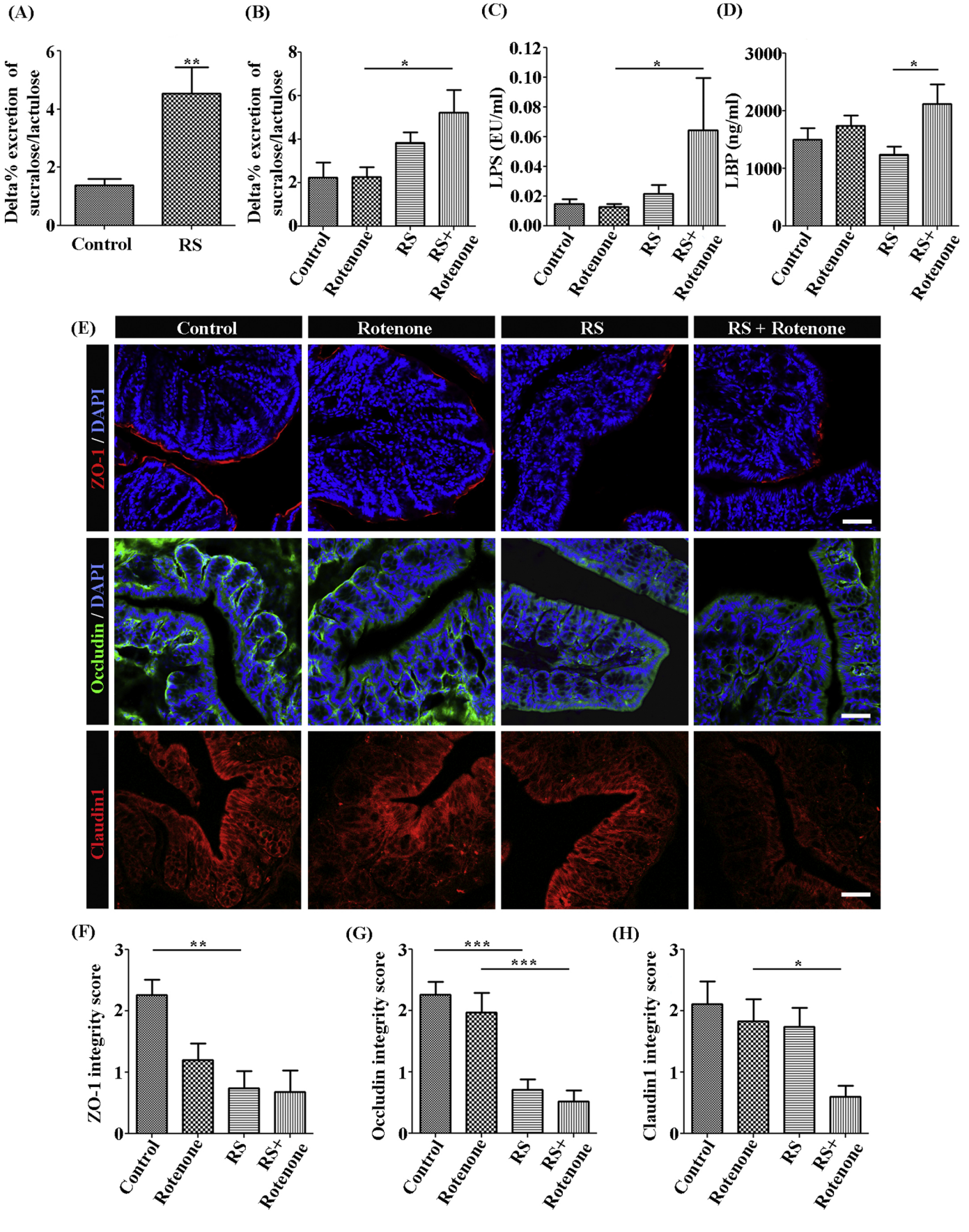
(A)
Delta% excretion of sucralose/lactulose
Control
RS
(B)
Delta% excretion of sucralose/lactulose
Control
Rotenone
RS
RS+ Rotenone
(C)
LPS (EU/ml)
(D)
LBP (ng/ml)
(E)
Control
Rotenone
RS
RS + Rotenone
ZO-1 / DAPI
Occludin / DAPI
Claudin1
(F)
ZO-1 integrity score
(G)
Occludin integrity score
(H)
Claudin1 integrity score

Figure 2

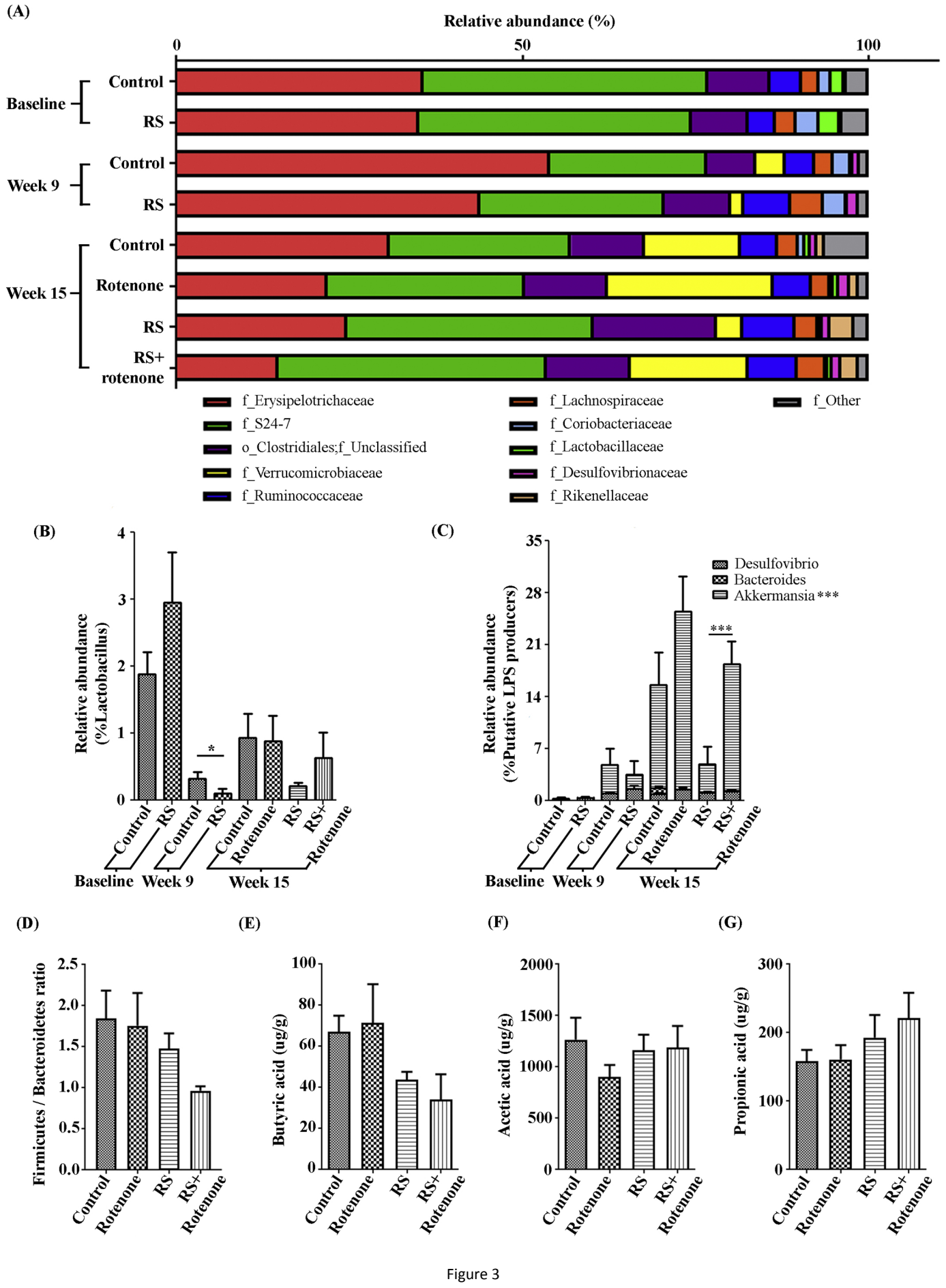
(A)
Relative abundance (%)
0
50
100
Baseline
Control
RS
Week 9
Control
RS
Week 15
Control
Rotenone
RS
RS+ rotenone
f_Erysipelotrichaceae
f_S24-7
o_Clostridiales;f_Unclassified
f_Verrucomicrobiaceae
f_Ruminococcaceae
f_Lachnospiraceae
f_Coriobacteriaceae
f_Lactobacillaceae
f_Desulfovibrionaceae
f_Rikenellaceae
f_Other
(B)
Relative abundance (%Lactobacillus)
*
Control
RS
Control
RS
Control
Rotenone
RS
RS+ Rotenone
Baseline
Week 9
Week 15
(C)
Relative abundance (%Putative LPS producers)
Desulfovibrio
Bacteroides
Akkermansia ***
***
Control
RS
Control
RS
Control
Rotenone
RS
RS+ Rotenone
Baseline
Week 9
Week 15
(D)
Firmicutes / Bacteroidetes ratio
Control
Rotenone
RS
RS+ Rotenone
(E)
Butyric acid (ug/g)
Control
Rotenone
RS
RS+ Rotenone
(F)
Acetic acid (ug/g)
Control
Rotenone
RS
RS+ Rotenone
(G)
Propionic acid (ug/g)
Control
Rotenone
RS
RS+ Rotenone

Figure 3

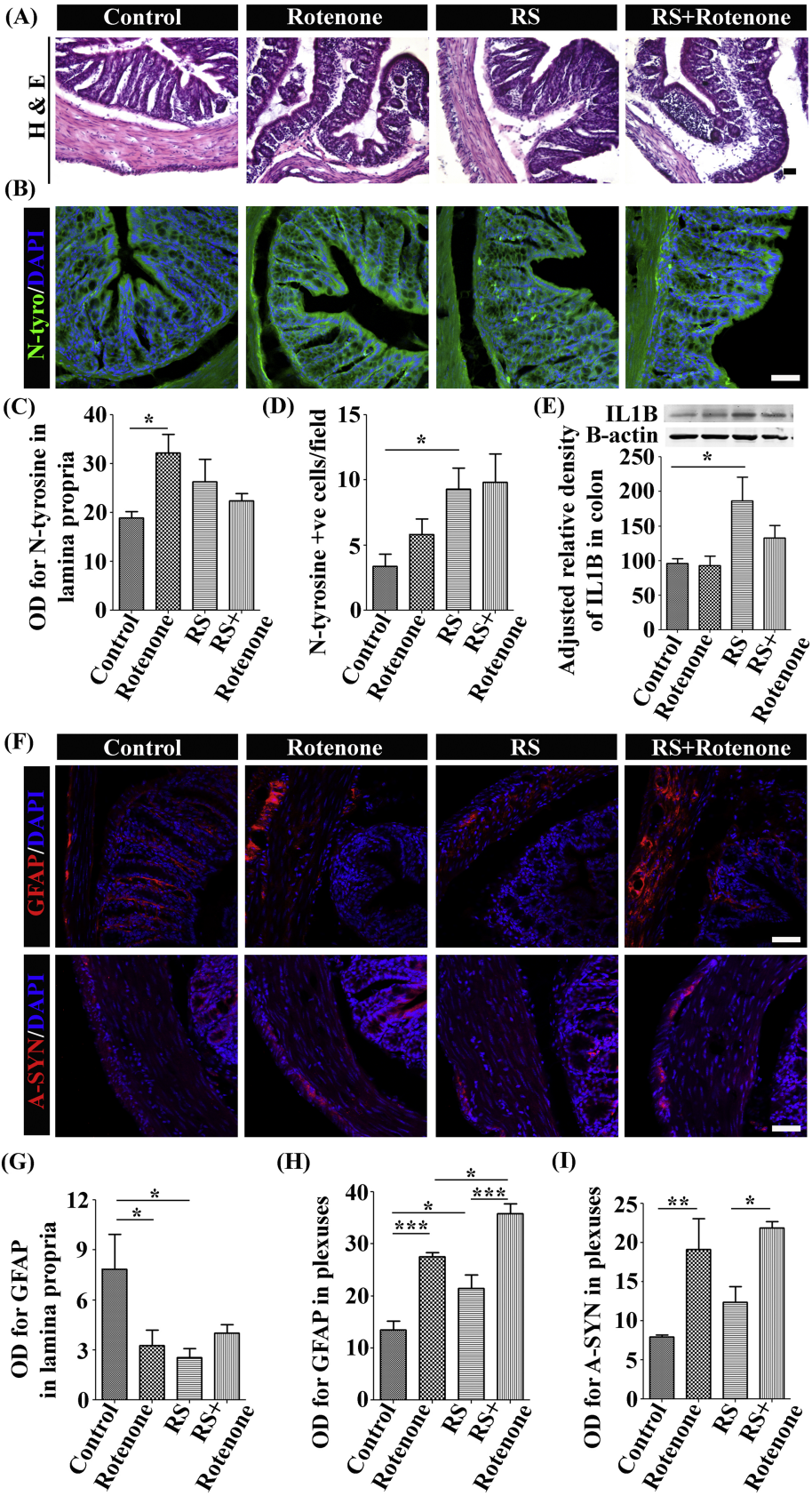
(A)
Control
Rotenone
RS
RS+Rotenone
H & E
(B)
N-tyro/DAPI
(C)
OD for N-tyrosine in lamina propria
40
30
20
10
0
*
Control
Rotenone
RS
RS+ Rotenone
(D)
N-tyrosine +ve cells/field
15
10
5
0
*
Control
Rotenone
RS
RS+ Rotenone
(E)
IL1B
B-actin
Adjusted relative density of IL1B in colon
250
200
150
100
50
0
*
Control
Rotenone
RS
RS+ Rotenone
(F)
Control
Rotenone
RS
RS+Rotenone
GFAP/DAPI
A-SYN/DAPI
(G)
OD for GFAP in lamina propria
12
9
6
3
0
*
*
Control
Rotenone
RS
RS+ Rotenone
(H)
OD for GFAP in plexuses
40
30
20
10
0
*
***
*
***
Control
Rotenone
RS
RS+ Rotenone
(I)
OD for A-SYN in plexuses
25
20
15
10
5
0
**
*
Control
Rotenone
RS
RS+ Rotenone

Figure 4

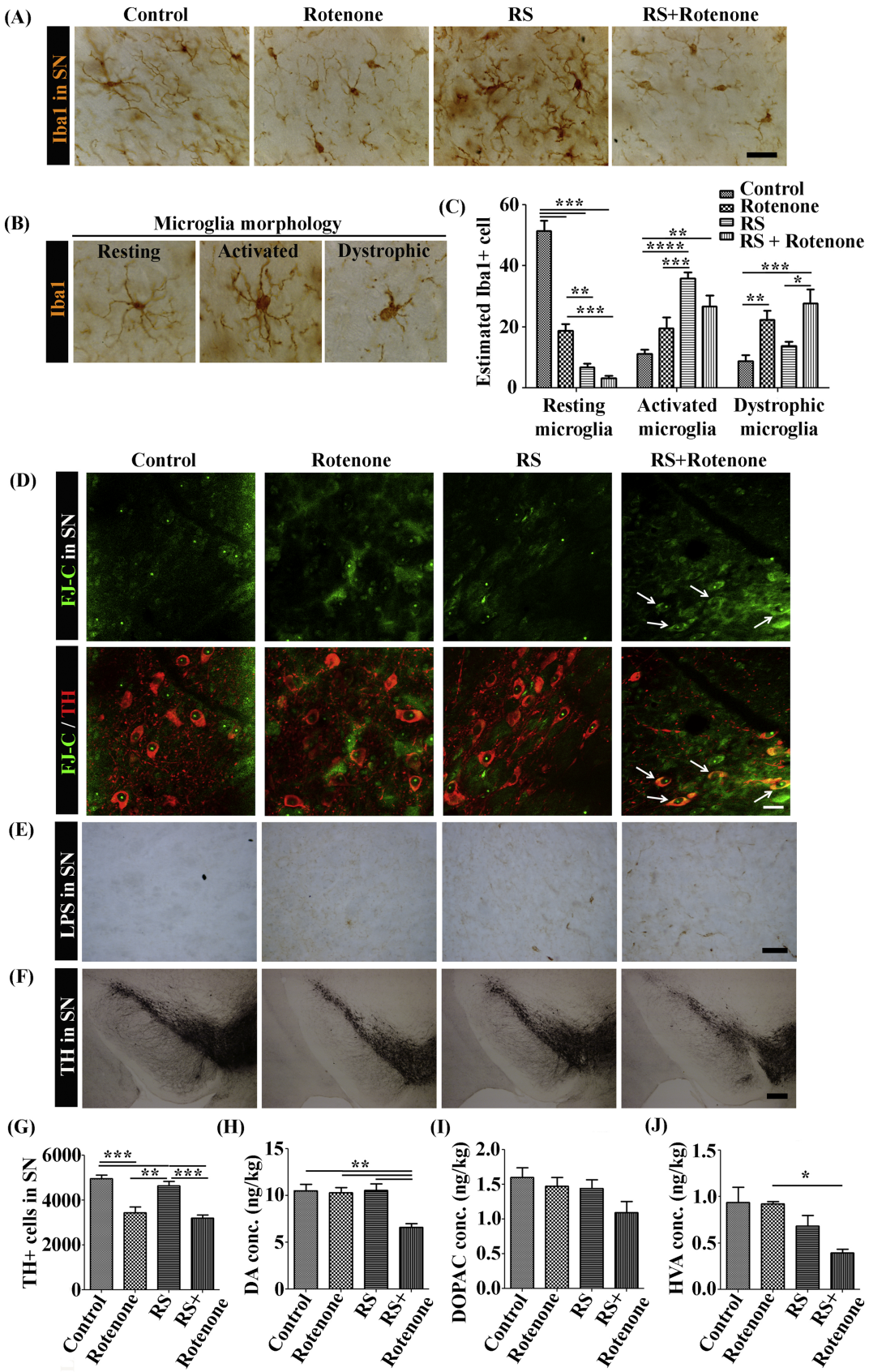
(A)
Control
Rotenone
RS
RS+Rotenone
Iba1 in SN
(B)
Microglia morphology
Iba1
Resting
Activated
Dystrophic
(C)
Control
Rotenone
RS
RS + Rotenone
Estimated Iba1+ cell
60
40
20
0
***
**
***
**
****
***
***
**
***
*
Resting microglia
Activated microglia
Dystrophic microglia
(D)
Control
Rotenone
RS
RS+Rotenone
FJ-C in SN
FJ-C / TH
(E)
LPS in SN
(F)
TH in SN
(G)
TH+ cells in SN
6000
4000
2000
0
***
**
***
Control
Rotenone
RS
RS+ Rotenone
(H)
DA conc. (ng/kg)
15
10
5
0
**
Control
Rotenone
RS
RS+ Rotenone
(I)
DOPAC conc. (ng/kg)
2.0
1.5
1.0
0.5
0.0
Control
Rotenone
RS
RS+ Rotenone
(J)
HVA conc. (ng/kg)
1.5
1.0
0.5
0.0
*
Control
Rotenone
RS
RS+ Rotenone

Figure 5

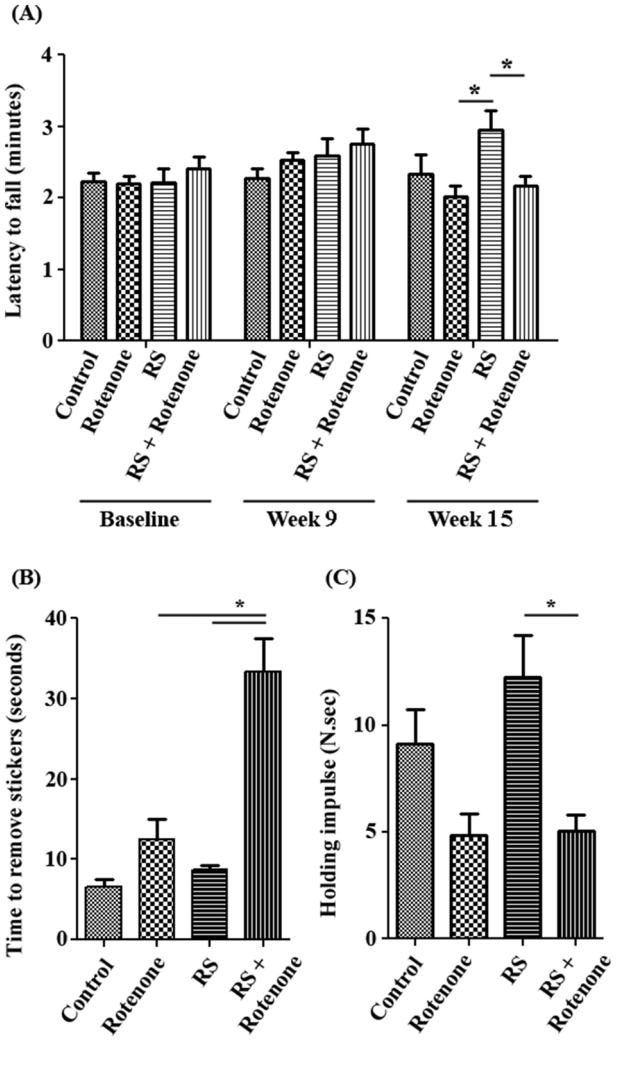
(A)
Latency to fall (minutes)
4
3
2
1
0
*
*
Control
Rotenone
RS
RS + Rotenone
Control
Rotenone
RS
RS + Rotenone
Control
Rotenone
RS
RS + Rotenone
Baseline
Week 9
Week 15
(B)
Time to remove stickers (seconds)
40
30
20
10
0
*
Control
Rotenone
RS
RS+ Rotenone
(C)
Holding impulse (N.sec)
15
10
5
0
*
Control
Rotenone
RS
RS+ Rotenone

Figure 6

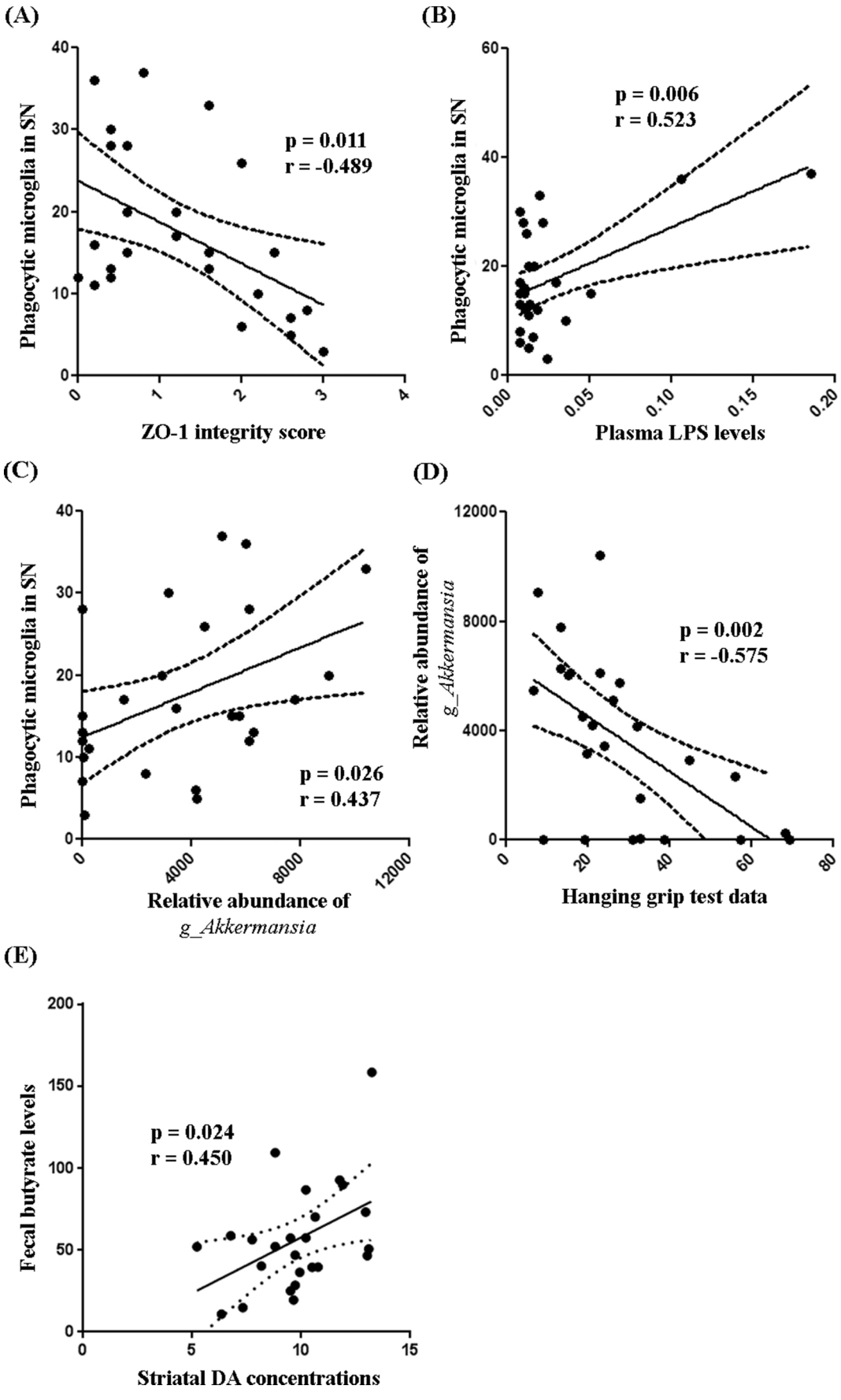
(A)
Phagocytic microglia in SN
p = 0.011
r = -0.489
ZO-1 integrity score
(B)
Phagocytic microglia in SN
p = 0.006
r = 0.523
Plasma LPS levels
(C)
Phagocytic microglia in SN
p = 0.026
r = 0.437
Relative abundance of
g_Akkermansia
(D)
Relative abundance of
g_Akkermansia
p = 0.002
r = -0.575
Hanging grip test data
(E)
Fecal butyrate levels
p = 0.024
r = 0.450
Striatal DA concentrations

Figure 7

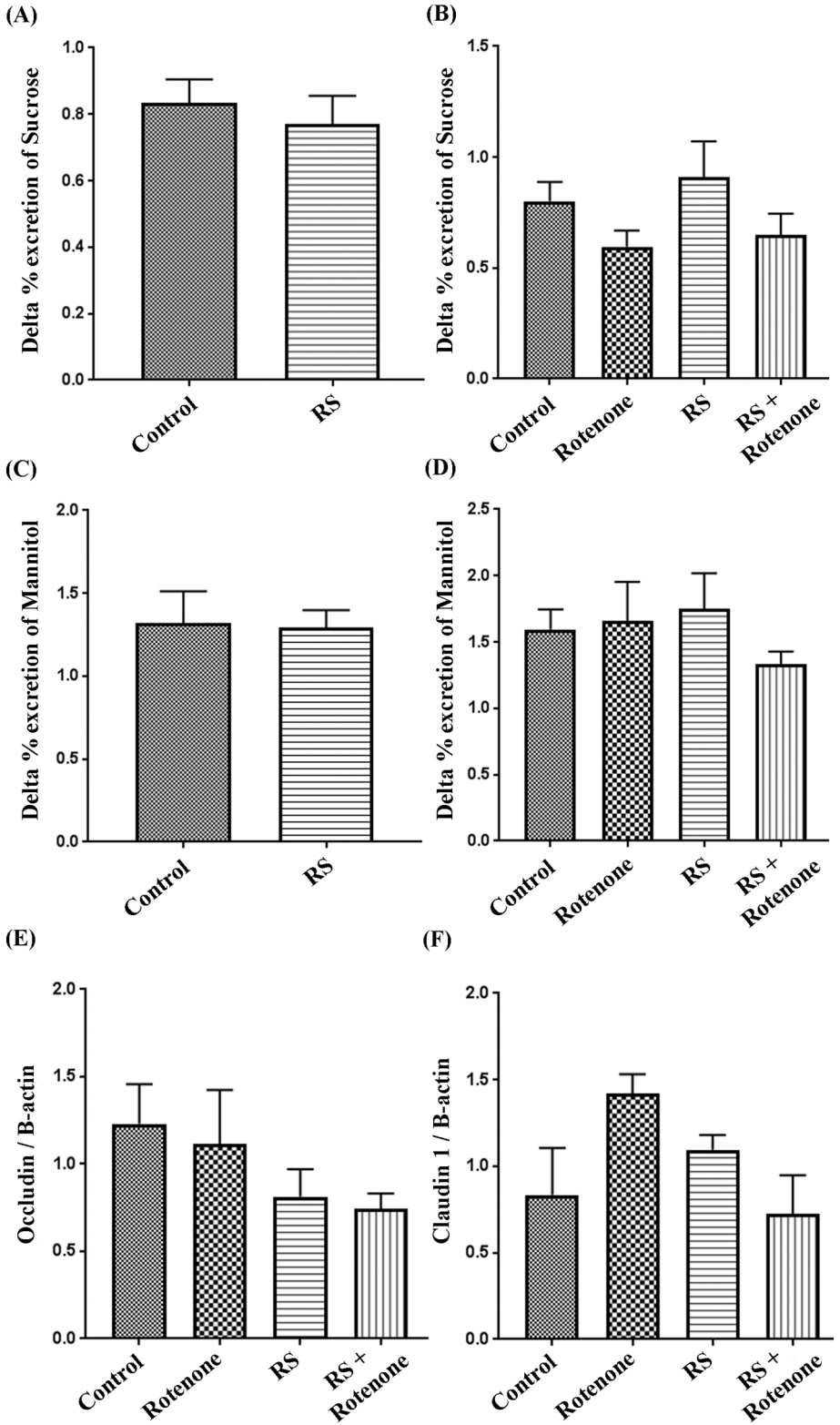
(A)
Delta % excretion of Sucrose
1.0
0.8
0.6
0.4
0.2
0.0
Control
RS
(B)
Delta % excretion of Sucrose
1.5
1.0
0.5
0.0
Control
Rotenone
RS
RS + Rotenone
(C)
Delta % excretion of Mannitol
2.0
1.5
1.0
0.5
0.0
Control
RS
(D)
Delta % excretion of Mannitol
2.5
2.0
1.5
1.0
0.5
0.0
Control
Rotenone
RS
RS + Rotenone
(E)
Occludin / B-actin
2.0
1.5
1.0
0.5
0.0
Control
Rotenone
RS
RS + Rotenone
(F)
Claudin 1 / B-actin
2.0
1.5
1.0
0.5
0.0
Control
Rotenone
RS
RS + Rotenone

Figure 8

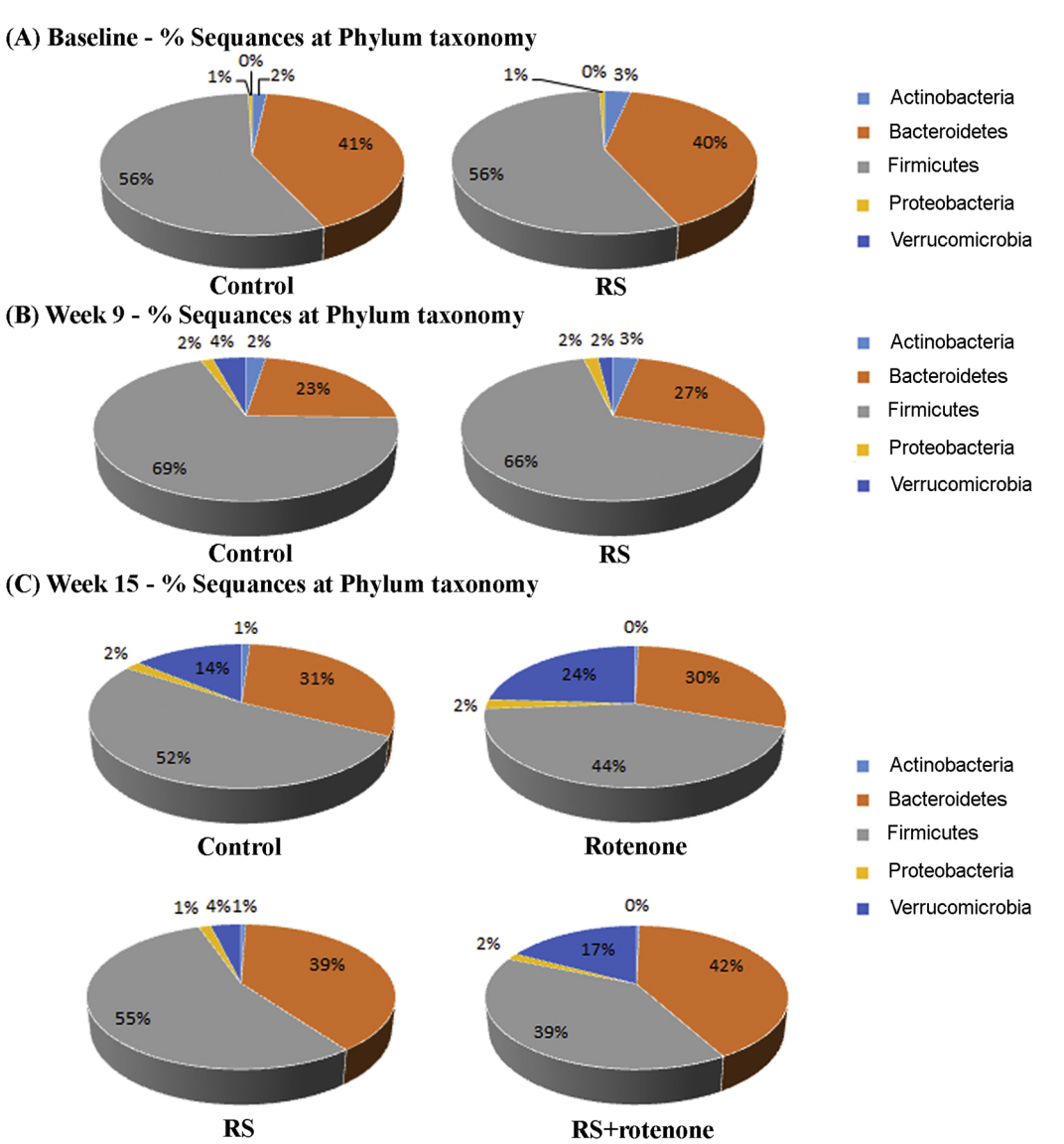

(D) Alpha diversity at Phylum taxonomy

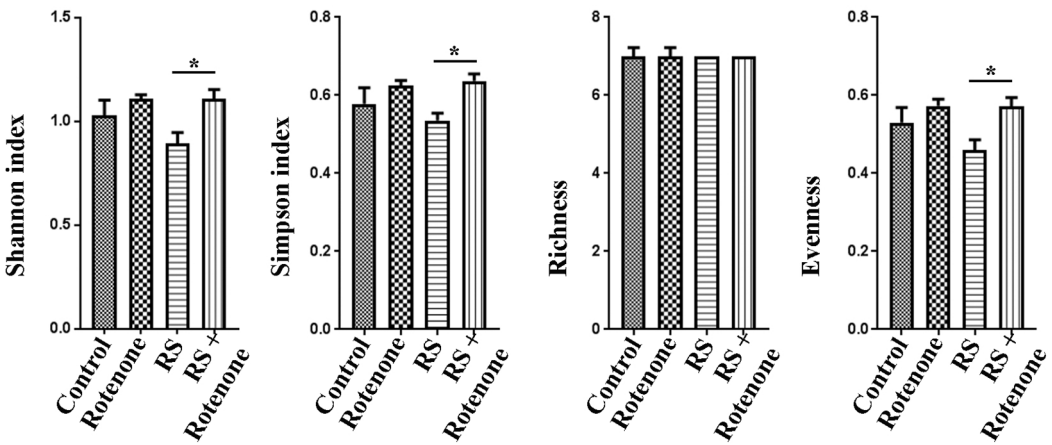

Figure 9

(A) Representative cytokine array blots

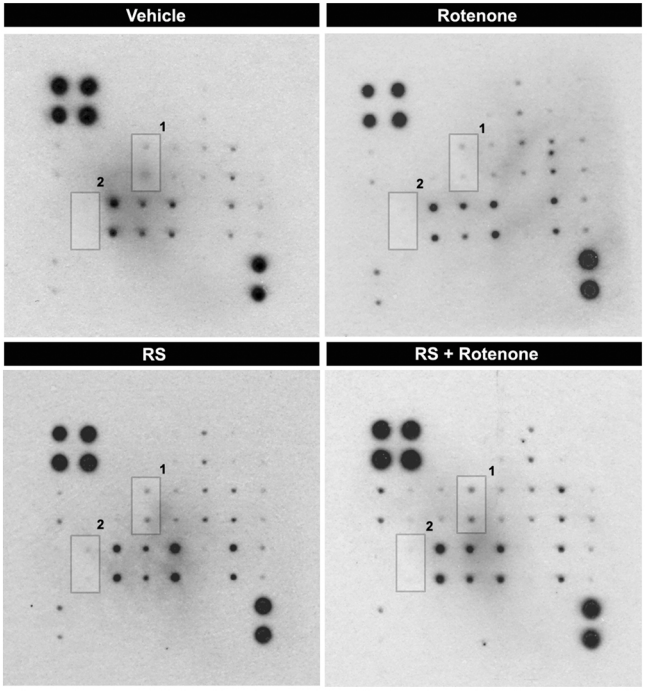

(B) Heatmap of Log2-noramlized cytokine array OD data

-7.51	-5.46	-3.88	-4.71	-5.25	-2.48	-2.16	-4.52	GCSF
-4.88	-5.33	-2.28	-5.79	9.76	-3.03	-1.75	-3.32	GM-CSF
-6.97	-7.72	-3.24		-7.20	-7.26	-2.77	-6.37	IL-2
-8.38		-3.07	-6.51	-8.42		-4.30	-7.11	IL-3
-6.11	-3.78	-4.20	-3.33	-3.50	-2.87	-2.34	11.13	IL-4
-8.97	-3.01	-6.40	-3.07	-4.85	-2.24	-2.40	-3.58	IL-5
-6.88	-2.25	-4.14	-2.41	-3.71	-1.80	-1.75	-2.64	IL-6
-3.57	-1.61	-2.49	-1.82	11.20	13.09	-0.77	9.83	IL-9 * 1
-3.77	-2.66	-1.98	-2.31	-2.15	10.60	15.88	-2.56	IL-10
-3.58	-3.39	12.58	-2.81	12.80	11.91	16.56	8.51	IL-12 p40/p70
8.36	-3.04	14.21	-3.39	13.21	12.96	14.96	13.02	IL-12 p70
-5.11	-5.16	-2.00	-4.06	-4.46	-3.96	-1.21	-3.91	IL-13
-7.51	-4.66	-5.26	-3.33	-4.94	-4.80	-6.34	-7.43	IL-17A
-6.27	-5.18	-4.11	-2.58	-3.28	-2.57	-4.85	-4.73	IFN-gamma * 2
16.51	16.16	16.63	7.41	16.43	16.11	16.00	16.26	MCP-1 (CCL2)
15.34	-0.74	15.55	-1.30	15.17	16.32	14.56	15.32	MCP-5
12.37	12.90	16.74	6.42	17.31	17.20	14.65	15.23	RANTES (CCL5)
-4.06	-3.74	-2.09	-2.37	-2.95	-2.34	-0.51	-3.99	SCF
14.55	-2.75	16.13	-1.74	15.93	9.93	15.45	13.49	TNF RI (TNFRSF1A)
-4.61	-3.84	-1.76	-3.65	-3.82	-3.69	8.79	-4.18	TNF-alpha
-4.56	-4.51	11.42	-5.28	9.44	-4.98		-5.43	TPO
-7.06	-5.24	-7.72	-6.03		-4.82	-6.13		VEGF-A
1	2	1	2	1	2	1	2	
Control		Rotenone		RS		RS + Rotenone		

(C) Cytokine antibody layout

	A	B	C	D	E	F	G	H
1	POS	POS	NEG	NEG	GCSF	GM-CSF	IL-2	IL-3
2								
3	IL-4	IL-5	IL-6	IL-9	IL-10	IL-12 p40/p70	IL-12 p70	IL-13
4								
5	IL-17A	IFN-gamma	MCP-1 (CCL2)	MCP-5	RANTES (CCL5)	SCF	TNF RI (TNFRSF1A)	TNF alpha
6								
7	TPO	VEGF-A	BLANK	BLANK	BLANK	BLANK	BLANK	POS
8								

Figure 10

(A) Rotenone standard curve

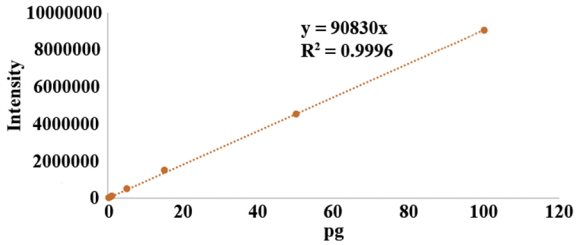

(B) a. Optimized MS conditions

Compound	MRM Q1/Q3	CE	DP
Rotenone	395/192	31	100
	395/213	30	100

b. Precision of the method

Analyte	R	LOD (fg)**	LOQ (fg)**
Rotenone	0.9996	20	100

(C) LC/MS spectrum of rotenone at 200fg

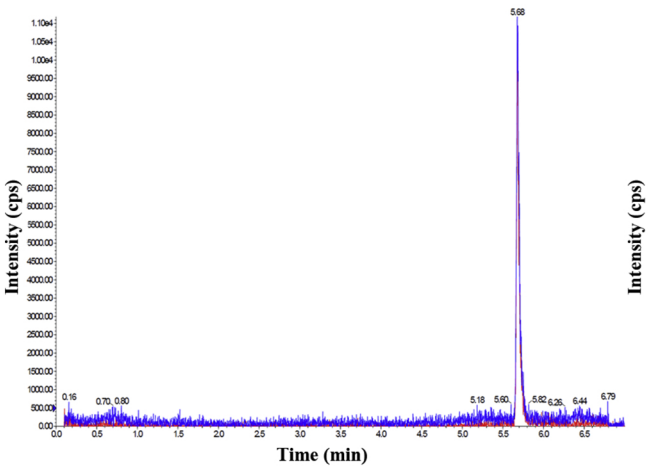

(D) LC/MS spectrum of rotenone spiked brain

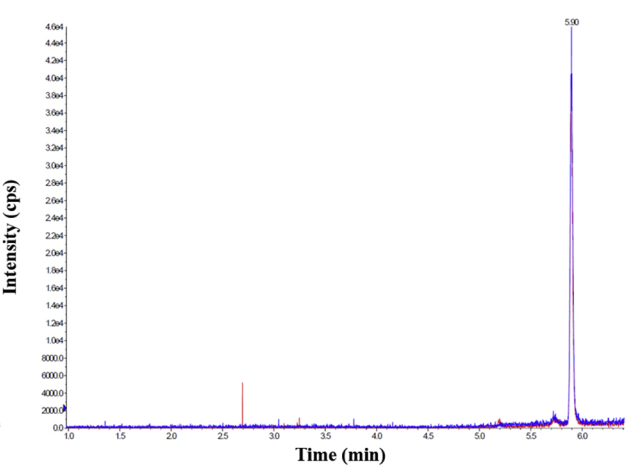

(E) LC/MS spectrum of saline spiked brain

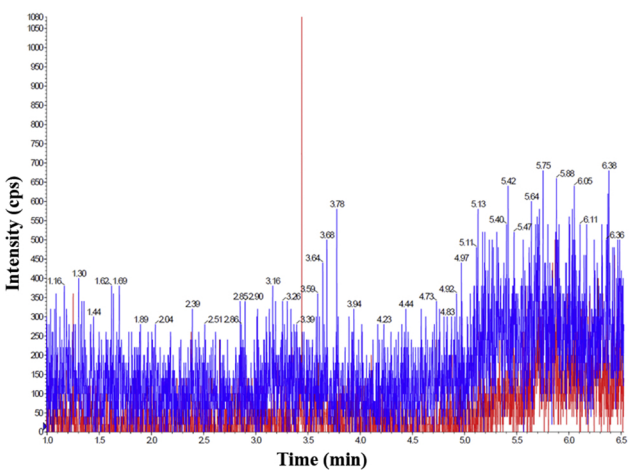

(F) LC/MS spectrum of Rotenone group mice brain

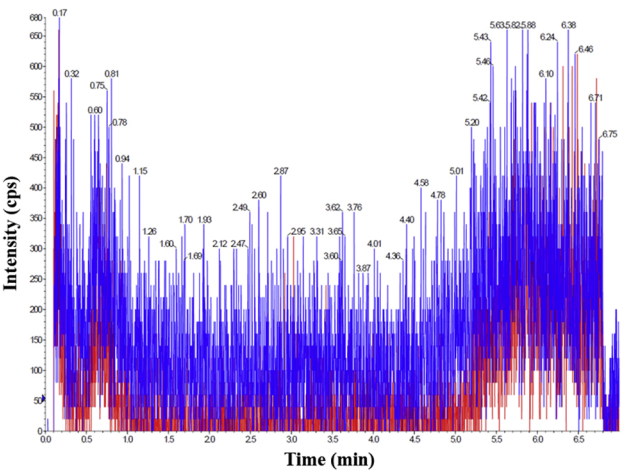

(G) LC/MS spectrum of RS+rotenone group mice brain

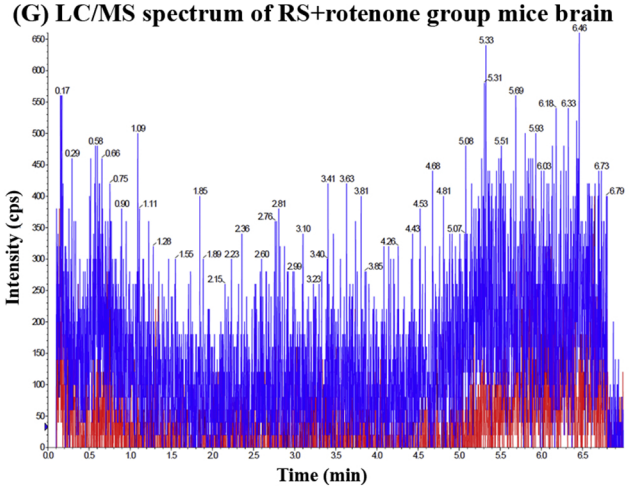

Figure 11

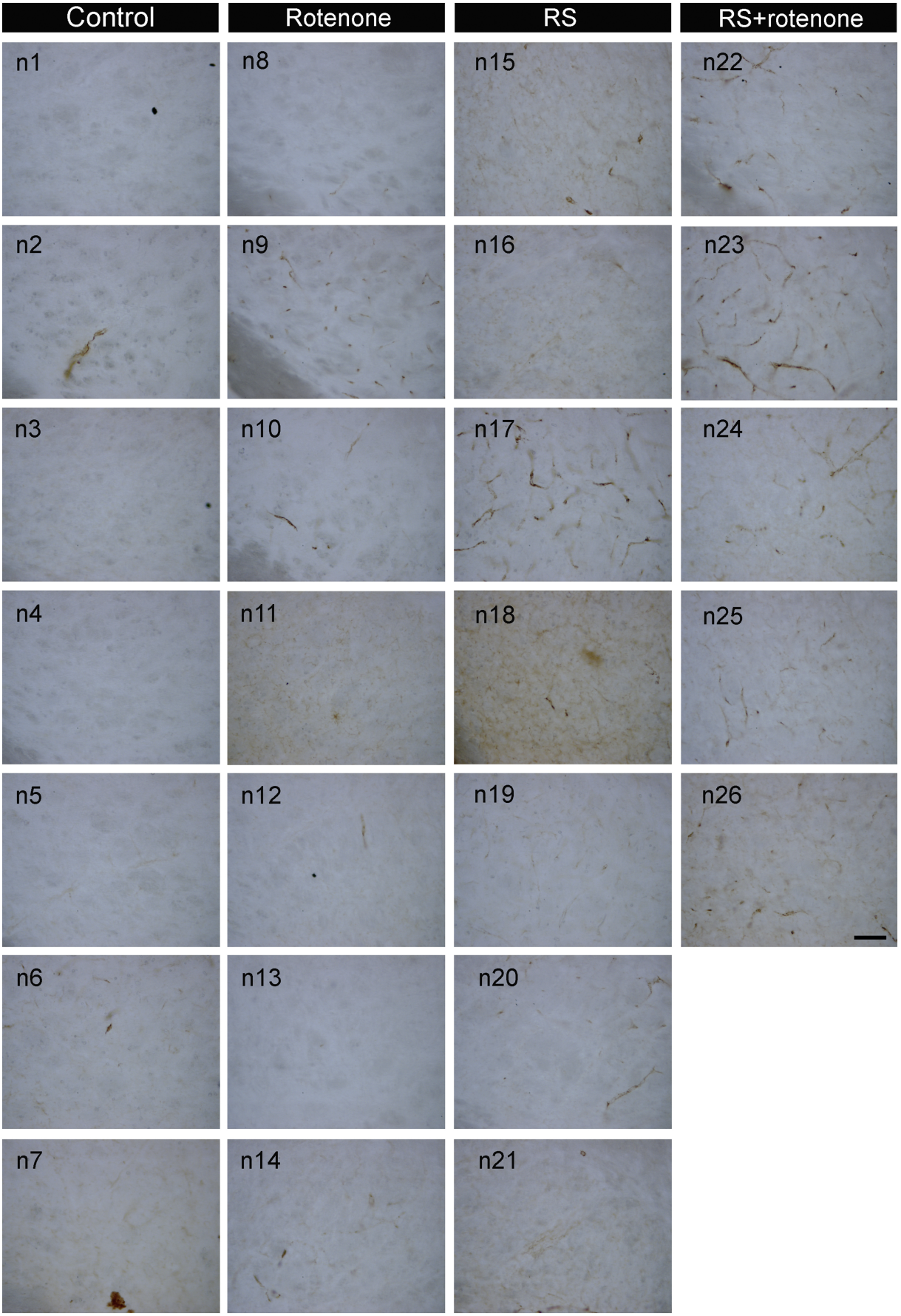
Control
Rotenone
RS
RS+rotenone
n1
n8
n15
n22
n2
n9
n16
n23
n3
n10
n17
n24
n4
n11
n18
n25
n5
n12
n19
n26
n6
n13
n20
n7
n14
n21

Figure 12

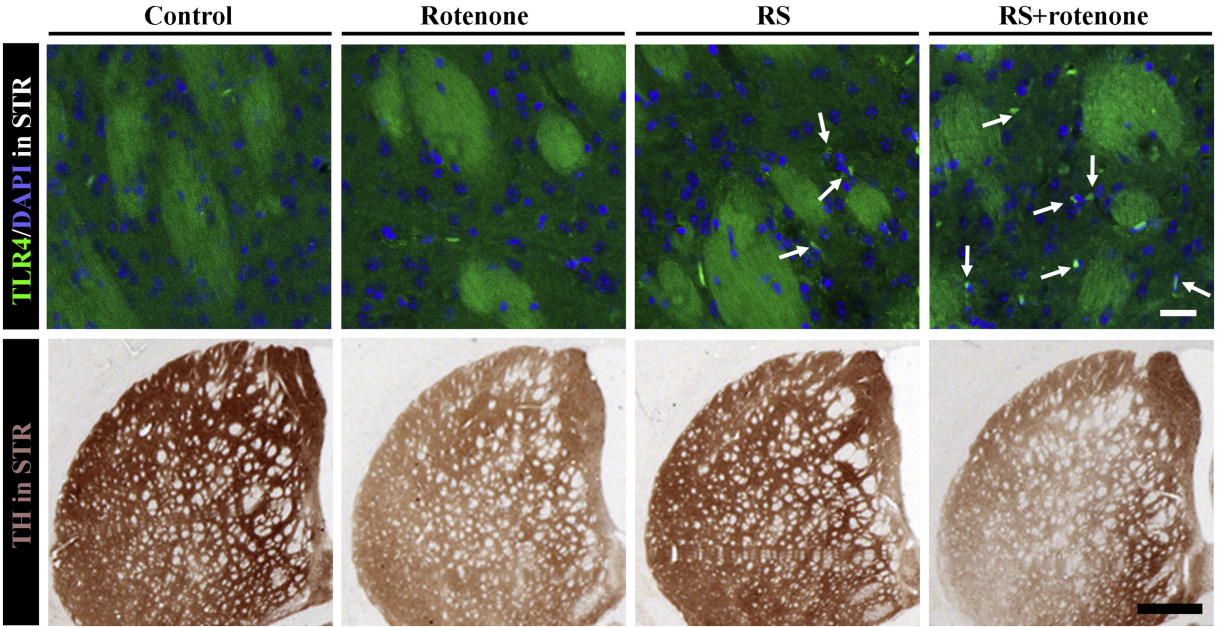

Figure 13